SIAM J. Appl. Math.
Vol. 75, No. 4, pp. 1817–1851

BOUNDARY LAYERS IN PRESSURE-DRIVEN FLOW IN SMECTIC A LIQUID CRYSTALS*

I. W. STEWART†, M. VYNNYCKY‡, S. MCKEE†, AND M. F. TOMÉ§

Abstract. This article examines the steady flow of a smectic A liquid crystal sample that is initially aligned in a classical "bookshelf" geometry confined between parallel plates and is then subjected to a lateral pressure gradient which is perpendicular to the initial local smectic layer arrangement. The nonlinear dynamic equations are derived. These equations can be linearized and solved exactly to reveal two characteristic length scales that can be identified in terms of the material parameters and reflect the boundary layer behavior of the velocity and the director and smectic layer normal orientations. The asymptotic properties of the nonlinear equations are then investigated to find that these length scales apparently manifest themselves in various aspects of the solutions to the nonlinear steady state equations, especially in the separation between the orientations of the director and smectic layer normal. Non-Newtonian plug-like flow occurs and the solutions for the director profile and smectic layer normal share features identified elsewhere in static liquid crystal configurations. Comparisons with numerical solutions of the nonlinear equations are also made.

Key words. smectic A liquid crystals, flow dynamics, continuum theory, analytic solution

AMS subject classifications. 35Gxx, 65Nxx, 76A15, 76A05, 76Dxx, 76Rxx

DOI. 10.1137/140983483

1. Introduction.

Nematic liquid crystals generally consist of elongated rod-like molecules that have a preferred local average direction. A unit vector **n**, called the director, is introduced to describe this average direction of the molecular alignment. Smectic liquid crystals are more ordered than nematics and, for many materials, the smectic phases occur at a temperature below that for which the same material exhibits the nematic phase. The smectic A (SmA) liquid crystal phase occurs when the molecules are arranged within parallel layers where the director is commonly aligned perpendicular to the layers and parallel to the local unit layer normal, **a**, as shown in Figure 1(a). Further details on the physics of liquid crystals can be found in the books by Chandrasekhar [8] and de Gennes and Prost [12], while more mathematical treatments can be found in the books by Stewart [31] and Virga [35].

The aforementioned depiction of SmA liquid crystals is a rather idealized version of this phase and the model used below will allow for discrepancies between the orientation of the director and the normal to the smectic layers, as shown schematically in Figure 1(b). This is especially relevant in flow problems where the layer normal

*Received by the editors August 22, 2014; accepted for publication (in revised form) June 12, 2015; published electronically August 26, 2015. This work is part of the activities developed within the CEPID-CeMEAI FAPESP project grant 2013/07375-0.

http://www.siam.org/journals/siap/75-4/98348.html

†Department of Mathematics and Statistics, University of Strathclyde, Livingstone Tower, 26 Richmond Street, Glasgow, G1 1XH, United Kingdom (i.w.stewart@strath.ac.uk, s.mckee@strath.ac.uk). The third author's work was supported by a travel assistance grant from the Royal Society of Edinburgh.

‡Division of Casting of Metals, Department of Materials Science and Engineering, Royal Institute of Technology (KTH), Brinellvägen 23, SE-10044 Stockholm, Sweden (michaelv@kth.se). This author's work was supported by a visiting researcher grant within the Government of Brazil's "Science without Borders" program.

§Departamento de Matemática Aplicada e Estatística, Instituto de Ciências Matemáticas e Computação, Universidade de São Paulo, São Carlos, SP, Brazil (murilo@icmc.usp.br). This author's work was supported by CNPq–Conselho Nacional de Desenvolvimento Científico e Tecnológico, grant 302631/2010-0.

need not necessarily coincide everywhere with the director. A separation between the director and layer normal was considered by Ribotta and Durand [27] and this, together with the sources mentioned in the next section, motivated the nonlinear dynamic continuum theory introduced by Stewart [33] that will be deployed in the problem to be investigated in this article. We consider a sample of SmA liquid crystal confined by fixed parallel planar plates separated at a distance d apart in a bookshelf-type geometry, as shown in Figure 2(a). This figure depicts the anticipated steady state smectic layer structure when a constant pressure gradient is applied in the x-direction, as has been discussed by de Gennes [11] and de Gennes and Prost [12, p. 431] for linearized model equations in the case when $\mathbf{n}$ and $\mathbf{a}$ are constrained to coincide. Indeed, de Gennes sketches the flow field (see Figure 2(c) and Figure 2(a) in [11]) and argues that the velocity, u, normal to the layers is given by

$$u(z) = -\lambda_p \frac{\partial p}{\partial x}\left(1 - \frac{\cosh(\kappa z)}{\sinh(\kappa L)}\right), \tag{1.1}$$

where λ_p is the permeation coefficient, $2L$ is the plate separation distance, and $\kappa = 1/\sqrt{\eta\lambda_p}$, where κ is comparable to the smectic interlayer distance (in the range $20 \sim 80$ Å) and η is the "one-constant" approximation of the viscosity. The purpose of this paper is to clarify and quantify what exactly is happening in this pressure-driven flow when $\mathbf{n}$ and $\mathbf{a}$ are anchored at the plates. It will transpire that not only does the boundary layer anticipated by de Gennes [11] exist, but another, considerably smaller one affecting $\mathbf{n}$ and $\mathbf{a}$ also exists; furthermore, it will be shown that these phenomena are particularly sensitive to changes in the magnitudes of the material parameters. Such effects have been reported by experimentalists [5, 6] but it has not previously been possible to capture their qualitative features via previous restricted linear model equations in which $\mathbf{n}$ and $\mathbf{a}$ always coincide. We shall demonstrate how this can be achieved and we shall provide a comprehensive asymptotic analysis of the nonlinear equations; these will be verified and made more precise through numerical computation.

The paper is organized as follows. Section 2 summarizes the dynamic theory, provides a mathematical description of the pressure-driven flow problem, and derives the governing nonlinear dynamic equations. These nonlinear equations are first linearized in section 3 in order to gain a preliminary insight into the steady state problem. It turns out that these equations can be solved exactly for all material parameters; moreover, two physically relevant length scales, given in (3.22) below, can be identified precisely in terms of the material parameters. These length scales will be shown to be directly related to the magnitudes of two physically important boundary layer "distances," which are in turn connected to the relative reorientations of $\mathbf{n}$ and $\mathbf{a}$ and the classical boundary layer "displacement thickness" in relation to the velocity profile. A plug-like flow profile occurs in the solution for the velocity. The results derived from the linearized equations allow appropriate rescaled quantities to be introduced and these enable the boundary layers to be estimated when asymptotic and numerical solutions to the nonlinear equations are sought in sections 4 and 5; comparisons between these results will be made and four distinct regions will be identified. The article closes in section 6 with a discussion.

2. Dynamic theory and description of the problem. The SmA dynamic theory of Stewart [33], which allows $\mathbf{n}$ and $\mathbf{a}$ to separate, will be summarized in section 2.1 before we go on to discuss, in section 2.2, the geometrical set-up and the particular model equations for a pressure-driven flow of SmA confined between

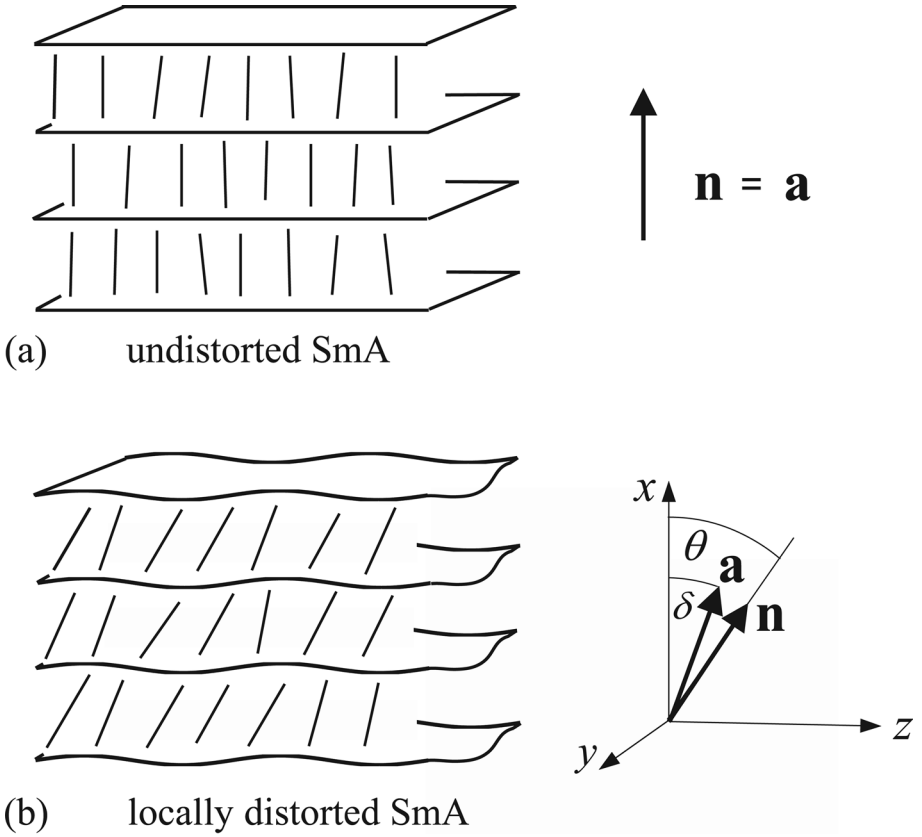

FIG. 1. (a) *A schematic diagram of locally arranged planar layers of SmA liquid crystal. In an undistorted configuration in the bulk, away from any boundary influences, the layers prefer to be equidistant and the local layer normal* **a** *coincides with the director* **n**. (b) *The layer and director alignments may be perturbed from their preferred undistorted orientations, in which case* **a** *and* **n** *need no longer coincide. The orientation angles* θ *and* δ*, for* **n** *and* **a***, respectively, are measured relative to the direction of the undistorted layer normal.*

two fixed parallel plates. It will be shown that there are three governing dynamic equations, given below by (2.29), (2.35), and (2.37), and it will be solutions to these equations that will be investigated subject to a symmetry requirement and suitable boundary conditions.

2.1. Dynamic theory. The dynamic theory for SmA liquid crystals formulated by Stewart [33] will be summarized briefly here. Cartesian tensor notation and the summation convention will be used so that any suffix that is repeated precisely twice in an expression is summed from 1 to 3. Partial differentiation with respect to the variable x_j is denoted by a subscript j preceded by a comma. Following the notation introduced in Figure 1, the smectic layer normal **a** is given by

$$a_i = \frac{\Phi_{,i}}{|\nabla\Phi|}\,, \qquad a_i a_i = 1\,, \tag{2.1}$$

where the smectic layers are modeled by the layer function Φ. The usual Oseen [24] constraint, $\nabla\times\mathbf{a} = \mathbf{0}$, a condition that is widely accepted for modeling the equilibrium structures of layered smectic phases in the absence of dislocations, will not be imposed

because small distortions to lamellar-like layer structures of SmA generally violate this condition.

The director $\mathbf{n}$ must satisfy the constraint

$$n_i n_i = 1\,, \tag{2.2}$$

and the incompressibility condition is given by

$$v_{i,i} = 0\,, \tag{2.3}$$

where $\mathbf{v}$ is the velocity. The rate of strain tensor A and vorticity tensor W are defined in the usual way by

$$A_{ij} = \tfrac{1}{2}(v_{i,j} + v_{j,i}), \qquad W_{ij} = \tfrac{1}{2}(v_{i,j} - v_{j,i}), \tag{2.4}$$

and, following the standard notation for nematics, the co-rotational time flux $\mathbf{N}$ of the director $\mathbf{n}$ is defined by

$$\mathbf{N} = \dot{\mathbf{n}} - \mathsf{W}\mathbf{n}\,. \tag{2.5}$$

A superposed dot represents the usual material time derivative given by

$$\frac{D}{Dt} = \frac{\partial}{\partial t} + v_i \frac{\partial}{\partial x_i}\,. \tag{2.6}$$

The general equations that arise from the balance law for linear momentum, in the absence of external body forces and generalized external body forces, are

$$\rho \dot{v}_i = -\tilde{p}_{,i} + \tilde{g}_j n_{j,i} + |\nabla\Phi| a_i J_{j,j} + \tilde{t}_{ij,j}\,, \tag{2.7}$$

where ρ is the density, $\tilde{p} = p + w_A$, where p is the pressure and w_A is the energy density, and $\mathbf{J}$ is a "phase flux" term defined by

$$J_i = -\frac{\partial w_A}{\partial\, \Phi_{,i}} + \frac{1}{|\nabla\Phi|}\left[\left(\frac{\partial w_A}{\partial a_{p,k}}\right)_{,k} - \frac{\partial w_A}{\partial a_p}\right](\delta_{pi} - a_p a_i)\,. \tag{2.8}$$

Note that $\mathbf{J}$ is a natural nonlinear extension to the versions discussed in [1, 2, 16, 11, 12]: when it is suitably linearized for small changes in the layer and director orientations, then it reduces to the explicit expressions found in [1, 2] when $\mathbf{n}$ and $\mathbf{a}$ are allowed to separate. It further reduces to the classical results in [12, 16] when $\mathbf{n} \equiv \mathbf{a}$. The constitutive equations for the viscous stress $\tilde{t}_{ij}$ and $\tilde{g}_i$ are, respectively,

$$\begin{aligned}
\tilde{t}_{ij} = {} & \alpha_1(n_k A_{kp} n_p) n_i n_j + \alpha_2 N_i n_j + \alpha_3 n_i N_j + \alpha_4 A_{ij} \\
& + \alpha_5(n_j A_{ip} n_p + n_i A_{jp} n_p) + (\alpha_2 + \alpha_3) n_i A_{jp} n_p \\
& + \tau_1(a_k A_{kp} a_p) a_i a_j + \tau_2(a_i A_{jp} a_p + a_j A_{ip} a_p) \\
& + \kappa_1(a_i N_j + a_j N_i + n_i A_{jp} a_p - n_j A_{ip} a_p) \\
& + \kappa_2(n_k A_{kp} a_p)(n_i a_j + a_i n_j) \\
& + \kappa_3[(n_k A_{kp} n_p) a_i a_j + (a_k A_{kp} a_p) n_i n_j] \\
& + \kappa_4[2(n_k A_{kp} a_p) n_i n_j + (n_k A_{kp} n_p)(a_i n_j + n_i a_j)] \\
& + \kappa_5[2(n_k A_{kp} a_p) a_i a_j + (a_k A_{kp} a_p)(n_i a_j + a_i n_j)] \\
& + \kappa_6(n_j A_{ip} a_p + n_i A_{jp} a_p + a_i A_{jp} n_p + a_j A_{ip} n_p)
\end{aligned} \tag{2.9}$$

and

$$\tilde{g}_i = -\gamma_1 N_i - \gamma_2 A_{ip} n_p - 2\kappa_1 A_{ip} a_p \,, \tag{2.10}$$

where

$$\gamma_1 = \alpha_3 - \alpha_2 \quad \text{and} \quad \gamma_2 = \alpha_2 + \alpha_3 \,. \tag{2.11}$$

The above coefficients α_1 to α_5, τ_1, τ_2 and κ_1 to κ_6 are dynamic viscosity coefficients. The viscosities α_1 to α_5 are nematic-like, while the three viscosities α_4, τ_1, and τ_2 are analogous to the classical incompressible SmA viscosities [16, equation (3.33)]; κ_1 to κ_6 are "coupling" viscosities that are related to the combined effects of nematic and SmA behavior. We remark here that a more extensive theory for SmC [22] has similar contributions.

The balance of angular momentum in the absence of generalized external body forces leads to the equations

$$\left(\frac{\partial w_A}{\partial n_{i,j}}\right)_{,j} - \frac{\partial w_A}{\partial n_i} + \tilde{g}_i = \mu n_i \,, \tag{2.12}$$

where μ is a Lagrange multiplier that arises from the constraint (2.2) and can usually be eliminated or evaluated by taking the scalar product of (2.12) with $\mathbf{n}$. The permeation equation is

$$\dot{\Phi} = -\lambda_p J_{i,i} \,, \tag{2.13}$$

where $\lambda_p \geq 0$ is the permeation coefficient. This links the layer flux through a stationary medium to the relevant thermodynamic force [12, 28]. Permeation in locally planar smectics can be thought of as a weak flow of material through the smectic layers in the direction of the local layer normal [20]. This idea was first introduced in the context of liquid crystals by Helfrich [18]. Equations (2.2), (2.3), (2.7), (2.12), and (2.13) provide nine equations in the nine unknowns Φ, n_i, v_i, p, and μ; the smectic layer normal $\mathbf{a}$ is, of course, determined by (2.1) from the solution for Φ.

One elementary candidate for an energy density is that used by Stewart [33], which has been based upon the one evidently first introduced by Ribotta and Durand [27] and other variants deployed in references [1, 2, 29, 33, 32, 30, 34, 13, 37, 38]. It is given by [33]

$$w_A = \tfrac{1}{2}K_1^n(\nabla\cdot\mathbf{n})^2 + \tfrac{1}{2}K_1^a(\nabla\cdot\mathbf{a})^2 + \tfrac{1}{2}B_0(\,|\nabla\Phi| + \mathbf{n}\cdot\mathbf{a} - 2)^2 + \tfrac{1}{2}B_1\big\{1 - (\mathbf{n}\cdot\mathbf{a})^2\big\} \,. \tag{2.14}$$

This energy density is invariant under the simultaneous changes in sign $\mathbf{n} \to -\mathbf{n}$ and $\mathbf{a} \to -\mathbf{a}$, which is equivalent to invariance under the simultaneous changes $\mathbf{n} \to -\mathbf{n}$ and $\nabla\Phi \to -\nabla\Phi$. The first term on the right-hand side of (2.14) represents the usual elastic splay deformation of the director $\mathbf{n}$, while the second term is a measure of the bending of the smectic layers; both K_1^n and K_1^a are positive elastic constants (measured in newtons). The third term represents smectic layer compression and originates from the classical descriptions of SmA liquid crystals [12, 16, 2]; B_0 is the positive layer compression constant. The fourth expression accounts for the strength of the coupling between $\mathbf{n}$ and $\mathbf{a}$ with the positive constant B_1 having the same dimensions as B_0 (energy per unit volume): in an equilibrium state this energy contribution is clearly minimized when $\mathbf{n}$ and $\mathbf{a}$ are parallel. This term can equally be written as $\frac{1}{2}B_1(\mathbf{n}\times\mathbf{a})^2$ since $\mathbf{n}$ and $\mathbf{a}$ are unit vectors, which is the form used

in [1, 2, 29]. Although B_1 has been investigated theoretically, measurements for it are scarce in the literature. Nevertheless, Ribotta and Durand [27] have estimated that $B_1 \lesssim B_0$. The coupling constant B_1 can alter the critical threshold for the onset of the classical Helfrich–Hurault effect (smectic layer undulations induced by a magnetic or electric field). This has been investigated by Stewart and Stewart [30], where it was shown that for small magnitudes of B_1 the critical field strength for the onset of this effect is lower than that for the classical case, which is recovered as this coupling constant increases: this is indicative of an increased coupling between **n** and **a**. The above model does not exclude the possibility that **n** and **a** may coincide at particular locations or regions.

The nonlinear steady state equations for pressure-driven channel flow will be derived in the next section. When this system of coupled equations is linearized, it turns out that it can be solved explicitly via the theory of linear ordinary differential equations: the most influential material parameters appear to be λ_p, K_1^n, and B_1, reflecting the importance of permeation, director distortions, and coupling of the layer orientation to the director; although B_0 appears in the nonlinear equations, this constant does not appear in the linear equations for a steady state pressure-driven flow. This is a direct consequence of the fact that the coefficient multiplying B_0 is not leading order. The linearized problem is solved in section 3. The solutions from the linear equations will be discussed in relation to known results in the literature. They can also be used for making appropriate comparisons with the asymptotic results and the numerically derived solutions to the nonlinear equations that are investigated in section 4.

2.2. Geometrical set-up and governing equations. Figure 2(a) represents a schematic diagram of a sample of SmA, bounded by planar boundary plates placed a distance d apart at $z = \pm d/2$, once a steady state has been reached under the influence of a pressure-driven flow in the x-direction. The orientations of **n** and **a** are described by the angles $\theta(z)$ and $\delta(z)$, respectively, measured relative to the horizontal x-axis, as shown in Figure 2(b). A non-Newtonian plug-like flow profile is anticipated, based on the earlier work by de Gennes [11], and this is pictured in the notional flow profile shown relative to the local smectic layer arrangement in Figure 2(c). The standard no-slip boundary conditions apply and the SmA layers and the director are assumed to be strongly anchored to the plates, in accordance with the boundary and symmetry conditions. It is therefore supposed that the velocity **v** is of the form

$$\mathbf{v} = (u(z), v(z), 0)\,, \tag{2.15}$$

where the possibility of a transverse flow component in the y-direction is included (a common phenomenon in nematic liquid crystals [31, 10]). The no-slip boundary conditions are

$$u(\pm d/2) = v(\pm d/2) = 0\,. \tag{2.16}$$

Strong anchoring of the director and the smectic layers leads to the boundary conditions

$$\theta(\pm d/2) = \pm\theta_0, \quad \delta(\pm d/2) = \pm\delta_0\,, \tag{2.17}$$

where we have, for the moment, supposed symmetrical alignments at the boundaries with positive values for θ_0 and δ_0. The anticipated symmetry of the steady state profile shows that there is an expected change in the concavity of δ at $z = 0$: as z

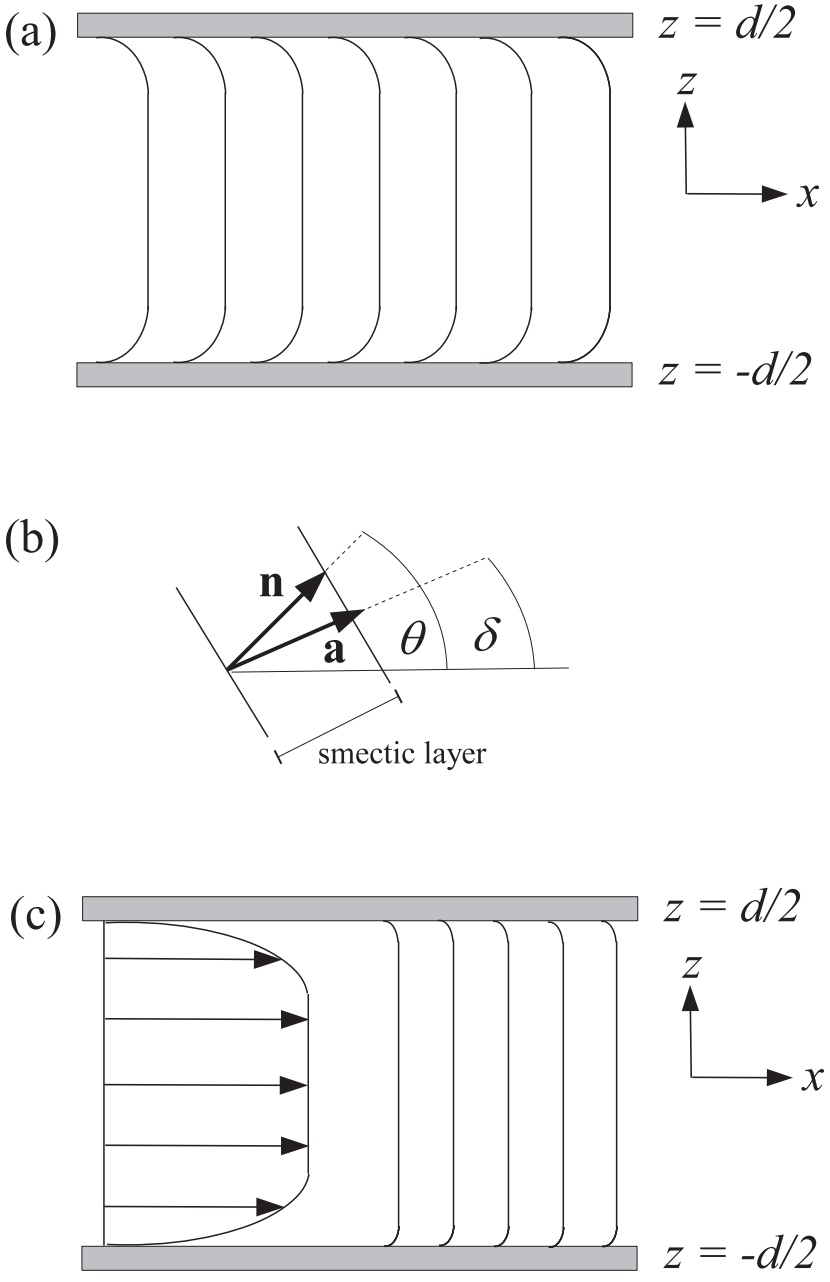

FIG. 2. (a) *A schematic illustration of the anticipated alignment of the SmA layers in a steady state situation when there is a pressure-driven flow in the x-direction. The liquid crystal is placed between two parallel fixed boundary plates located at* $z = \pm d/2$ *and the sample is assumed to be uniformly aligned in the y-direction. Boundary layers are expected to occur which will have a consequent effect upon the orientation of the SmA layers near the boundaries.* (b) *The local orientation angles of* $\mathbf{n}$ *and* $\mathbf{a}$ *in relation to the local smectic layer profile are described by* $\theta(z)$ *and* $\delta(z)$*, respectively, measured relative to the horizontal x-axis.* (c) *A diagram of the anticipated plug-like permeation flow normal to the smectic layers mentioned by de Gennes* [11]. *The velocity profile is expected to be relatively flat except near the boundary walls.*

increases through zero, its second derivative should change from negative to positive with $\delta''(0) = 0$ in the center of the sample, where a prime denotes differentiation with respect to z. We are then led to impose the interior symmetry condition

$$\delta''(0) = 0. \tag{2.18}$$

Although this requirement may seem unusual, it proves critical since it enables the solution of the coupled equations derived below. It is also appropriate, and not unexpected, that the third derivative of δ will appear naturally in the permeation equation (see (3.2)); as highlighted by de Gennes and Prost [12, p. 411], it is the presence of a third-order derivative that is responsible for the highly anisotropic behavior of such a system.

The director can be set as

$$\mathbf{n} = (\cos\theta, 0, \sin\theta). \tag{2.19}$$

Following the technique outlined by Walker [36], we can set the layer function Φ to be

$$\Phi(x, z) = x + \int_{-\frac{d}{2}}^{z} \tan(\delta(r))\, dr, \tag{2.20}$$

from which it is seen that $|\nabla\Phi| = \sec\delta$, provided $-\pi/2 < \delta < \pi/2$. Furthermore, from the definition in (2.1), it follows that

$$\mathbf{a} = (\cos\delta, 0, \sin\delta), \tag{2.21}$$

and, consequently, we have

$$\mathbf{n} \cdot \mathbf{a} = \cos(\theta - \delta). \tag{2.22}$$

Straightforward calculations reveal that $\mathbf{N}$ and $\tilde{\mathbf{g}}$, defined in (2.5) and (2.10), are given by

$$\mathbf{N} = \tfrac{1}{2}(u'\sin\theta, v'\sin\theta, -u'\cos\theta) \tag{2.23}$$

and

$$\begin{aligned}\tilde{\mathbf{g}} = {} & \tfrac{1}{2}\gamma_1(u'\sin\theta, v'\sin\theta, -u'\cos\theta) - \tfrac{1}{2}\gamma_2(u'\sin\theta, v'\sin\theta, u'\cos\theta) \\ & - \kappa_1(u'\sin\delta, v'\sin\delta, u'\cos\delta)\,.\end{aligned} \tag{2.24}$$

It proves convenient to first examine the equations that arise from the balance of angular momentum given in (2.12). Calculations using the above expressions show that they are

$$M(\theta, \delta)\cos\delta + \tilde{g}_1 = \mu\cos\theta, \tag{2.25}$$

$$v'\,[\,(\gamma_1 - \gamma_2)\sin\theta - \kappa_1\sin\delta\,] = 0, \tag{2.26}$$

$$M(\theta, \delta)\sin\delta + K_1^n\frac{d^2}{dz^2}\sin\theta + \tilde{g}_3 = \mu\sin\theta, \tag{2.27}$$

where, for notational convenience, the function M has been introduced as

$$M(\theta, \delta) = B_1\cos(\theta - \delta) - B_0[\,\sec\delta + \cos(\theta - \delta) - 2\,]\,. \tag{2.28}$$

Equation (2.26) cannot be satisfied for arbitrary nonzero boundary conditions imposed on θ and δ unless $v' \equiv 0$. Hence $v(z)$ must generally be a constant and this constant must be zero by the no-slip boundary conditions. There will therefore be no transverse flow in this problem and the velocity reduces to $\mathbf{v} = (u(z), 0, 0,)$. Equation (2.26) is then satisfied automatically. The Lagrange multiplier can be eliminated from the remaining two equations by multiplying (2.25) by $\sin\theta$ and (2.27) by $\cos\theta$ and subtracting the resulting expressions. This final step allows the angular momentum equations to reduce to the single equation given by

(2.29)
$$M(\theta,\delta)\sin(\theta-\delta) - K_1^n \cos\theta \frac{d^2}{dz^2}\sin\theta + \frac{du}{dz}\left[\,\alpha_3\cos^2\theta - \alpha_2\sin^2\theta + \kappa_1\cos(\theta-\delta)\,\right] = 0,$$

where use has been made of the relations in (2.11).

The divergence of $\mathbf{J}$ appears in the linear momentum and permeation equations: however, the evaluation of this divergence will only involve the derivative of the third component of $\mathbf{J}$ because of the assumed dependency on z and therefore only J_3 needs to be calculated explicitly. We have, from (2.8), that

(2.30)
$$J_3 = \cos^2\delta\left[K_1^a\cos\delta\frac{d^2}{dz^2}\sin\delta + M(\theta,\delta)\sin(\theta-\delta)\right] - B_0\sin\delta[\,\sec\delta + \cos(\theta-\delta) - 2\,].$$

Direct calculations reveal that $\rho\dot{\mathbf{v}} = \mathbf{0}$ and therefore the linear momentum equations (2.7) become, in an obvious notation,

$$p_{,x} = J_{3,3} + \tilde{t}_{13,3}\,, \tag{2.31}$$

$$p_{,y} = 0\,, \tag{2.32}$$

$$p_{,z} = -(w_A)_{,3} + \tilde{g}_j n_{j,3} + J_{3,3}\tan\delta + \tilde{t}_{33,3}\,. \tag{2.33}$$

The right-hand side of (2.33) is a function of z only and so we may abbreviate it as $G(z)$. Under the assumption that a constant pressure gradient, $a < 0$, is applied (so that the pressure induced flow is in the positive x-direction), we can identify the pressure from these equations as

$$p(x,z) = ax + \int_{-\frac{d}{2}}^{z} G(s)\,ds + p_0, \tag{2.34}$$

where p_0 is an arbitrary constant pressure. It is evident that this form for the pressure satisfies (2.32) and (2.33) and so these particular equations can be eliminated from the discussion. Insertion of $p(x,z)$ into (2.31) leads to

$$a = J_{3,3} + \tilde{t}_{13,3}\,, \tag{2.35}$$

which is the single equation that remains from the linear momentum equations. The only component of the viscous stress that needs to be evaluated explicitly is therefore $\tilde{t}_{13}$. Inserting $\mathbf{v}$, $\mathbf{n}$, and $\mathbf{a}$ into (2.4), (2.23), and (2.9) gives

$$\begin{aligned}\tilde{t}_{13} = {}& \tfrac{1}{2}u'\,(\alpha_4+\alpha_5-\alpha_2+\tau_2) + \tfrac{1}{4}u'\left[\,\alpha_1\sin^2(2\theta) + \tau_1\sin^2(2\delta)\,\right]\\ & + u'\left[\,\kappa_1\cos(\theta+\delta) + \kappa_6\cos(\theta-\delta) + (\alpha_2+\alpha_3)\cos^2\theta\,\right]\\ & + \tfrac{1}{2}u'\left[\,\kappa_2\sin^2(\theta+\delta) + \kappa_3\sin(2\theta)\sin(2\delta)\,\right]\\ & + u'\sin(\theta+\delta)\left[\,\kappa_4\sin(2\theta) + \kappa_5\sin(2\delta)\,\right].\end{aligned} \tag{2.36}$$

The results from (2.30) and (2.36) can be inserted into (2.35) when required for calculations.

It can be verified that the material derivative of Φ, defined in (2.20), with respect to the velocity $\mathbf{v} = (u, 0, 0)$ is $\dot{\Phi} = u$ and so the permeation equation (2.13) becomes

$$u + \lambda_p J_{3,3} = 0. \tag{2.37}$$

The three governing equations for this pressure-driven flow are given by (2.29), (2.35), and (2.37), subject to the boundary conditions (2.16), and (2.17) and the requirement (2.18). Before going on to solve these nonlinear equations, it is worth examining the linearized equations in order to identify any potential key material parameters to the problem that may be indicative of characteristic behavior on various length scales or ranges of parameters. The linear equations will be solved analytically to obtain exact solutions. This procedure will be carried out in the next section as a preliminary study prior to obtaining asymptotic and numerical solutions to the nonlinear equations that will be discussed in sections 4 and 5.

3. Linearized equations. Equations (2.29), (2.35), and (2.37) can be linearized under the assumption that the solutions u, θ, δ and their derivatives are small. This leads to the three equations

$$B_1(\theta - \delta) - K_1^n \theta'' + u'(\alpha_3 + \kappa_1) = 0, \tag{3.1}$$

$$K_1^a \delta''' + B_1(\theta' - \delta') + \eta u'' - a = 0, \tag{3.2}$$

$$u + \lambda_p \left[K_1^a \delta''' + B_1(\theta' - \delta') \right] = 0, \tag{3.3}$$

where, as an abbreviation, we have defined the viscosity coefficient η by

$$2\eta = \alpha_2 + \alpha_4 + \alpha_5 + \tau_2 + 2\left(\alpha_3 + \kappa_1 + \kappa_6\right). \tag{3.4}$$

The viscosity coefficients on the right-hand side of (3.4) tend to zero as the transition to an isotropic fluid takes place, except for the coefficient α_4: the reason for this is analogous to that for the case of smectic C liquid crystals [31, section 6.3.2]. Therefore in the isotropic limit, when $\mathbf{n}$ and $\mathbf{a}$ are absent, only the usual viscosity for a Newtonian fluid remains, namely, $\eta = \alpha_4/2$. This observation will be useful for making comparisons between the results that follow and the well-known results for isotropic fluids.

To simplify the presentation, the approximation $K_1^n = K_1^a$ will be used since these elastic constants can be considered as being of the same order of magnitude (cf. Auernhammer et al. [2]): the exact solutions can still be found when this approximation is not made but the results become unwieldy and tend to obscure the key roles of various material parameters. Notice also that, using (3.3), (3.2) can be rewritten as

$$\eta u'' - u\lambda_p^{-1} - a = 0\,. \tag{3.5}$$

The linear system of equations consisting of (3.1), (3.3), and (3.5) can then be written as a matrix system of the form

$$\frac{d\mathbf{x}}{dz} = A\mathbf{x} + \mathbf{b}\,, \tag{3.6}$$

where the column vectors $\mathbf{x}(z)$ and $\mathbf{b}$ are

$$\mathbf{x} = (\theta, \theta', \delta, \delta', \delta'', u, u')^{\mathrm{T}}, \qquad \mathbf{b} = (0, 0, 0, 0, 0, 0, a/\eta)^{\mathrm{T}}, \tag{3.7}$$

and A is the 7×7 constant coefficient matrix given by

(3.8)
$$A=\begin{bmatrix} 0 & 1 & 0 & 0 & 0 & 0 & 0 \\ B_1/K_1^a & 0 & -B_1/K_1^a & 0 & 0 & 0 & (\alpha_3+\kappa_1)/K_1^a \\ 0 & 0 & 0 & 1 & 0 & 0 & 0 \\ 0 & 0 & 0 & 0 & 1 & 0 & 0 \\ 0 & -B_1/K_1^a & 0 & B_1/K_1^a & 0 & -1/K_1^a\lambda_p & 0 \\ 0 & 0 & 0 & 0 & 0 & 0 & 1 \\ 0 & 0 & 0 & 0 & 0 & 1/\eta\lambda_p & 0 \end{bmatrix}.$$

The system (3.6) can be solved exactly. The eigenvalues of A are $\pm\lambda_1$, $\pm\lambda_2$, and zero, this latter eigenvalue having algebraic multiplicity three, where

$$\lambda_1=\frac{1}{\sqrt{\eta\lambda_p}}\,,\qquad \lambda_2=\sqrt{\frac{2B_1}{K_1^a}}\,. \tag{3.9}$$

The general solution of such a system with a repeated eigenvalue can be determined by constructing a suitable fundamental matrix $R(z)$ [40, p. 582]. The general solution is then

$$\mathbf{x}(z)=R(z)\,\mathbf{c}+R(z)\int^z R^{-1}(s)\,\mathbf{b}\,ds\,, \tag{3.10}$$

where $\mathbf{c}=(c_1,c_2,\ldots,c_7)^{\mathrm{T}}$ is a constant column vector. The seven components of this constant vector can be determined from the six boundary conditions contained in (2.16) and (2.17) and the requirement (2.18) (recall that $v(z)\equiv0$). Explicitly, we find that $R(z)=Q(z)\mathrm{diag}(e^{\lambda_1 z},e^{-\lambda_1 z},1,e^{\lambda_2 z},e^{-\lambda_2 z},1,1)$, where $Q(z)$ is the matrix

$$Q(z)=\begin{bmatrix} \beta_1 & \beta_1 & 1 & -1 & -1 & \frac{1}{2}z^2+z+1+2\lambda_2^{-2} & z+1 \\ \lambda_1\beta_1 & -\lambda_1\beta_1 & 0 & -\lambda_2 & \lambda_2 & z+1 & 1 \\ 1 & 1 & 1 & 1 & 1 & \frac{1}{2}z^2+z+1 & z+1 \\ \lambda_1 & -\lambda_1 & 0 & \lambda_2 & -\lambda_2 & z+1 & 1 \\ \lambda_1^2 & \lambda_1^2 & 0 & \lambda_2^2 & \lambda_2^2 & 1 & 0 \\ -\lambda_1^2\beta_2 & \lambda_1^2\beta_2 & 0 & 0 & 0 & 0 & 0 \\ -\lambda_1^3\beta_2 & -\lambda_1^3\beta_2 & 0 & 0 & 0 & 0 & 0 \end{bmatrix}, \tag{3.11}$$

and the constants β_1 and β_2 are defined by

$$\beta_1=\frac{[\,B_1\eta\lambda_p(\alpha_3+\kappa_1-\eta)-K_1^a(\alpha_3+\kappa_1)\,]}{\eta\,[\,K_1^a+B_1\lambda_p(\alpha_3+\kappa_1-\eta)\,]}\,, \tag{3.12}$$

$$\beta_2=\frac{(K_1^a)^2(\lambda_1^2-\lambda_2^2)}{\eta\lambda_1^3\,[\,K_1^a+B_1\lambda_p(\alpha_3+\kappa_1-\eta)\,]}\,. \tag{3.13}$$

Applying the conditions (2.16), (2.17), and (2.18) to the solution (3.10) shows that

$$c_2=-c_1,\quad c_3=-c_7,\quad c_5=-c_4,\quad c_6=0 \tag{3.14}$$

with

$$c_1 = -\frac{a\,\mathrm{sech}(\lambda_1 d/2)}{2\lambda_1^4 \eta \beta_2}\,, \tag{3.15}$$

$$c_4 = \frac{\mathrm{cosech}(\lambda_2 d/2)}{16 B_1 K_1^a \eta \lambda_p (\lambda_2^2 - \lambda_1^2)} \Big\{ \left[\, 4B_1(\delta_0 - \theta_0) + ad \,\right] \times (2B_1 \eta \lambda_p - K_1^a) - 4aB_1 \lambda_p^{\frac{3}{2}} \eta^{\frac{1}{2}} (\alpha_3 + \eta + \kappa_1) \tanh(\lambda_1 d/2) \Big\}\,, \tag{3.16}$$

$$c_7 = \frac{1}{d}(\delta_0 + \theta_0) - \frac{ad^2}{48 K_1^a} + \frac{a\lambda_p}{K_1^a d \lambda_1}(\eta - \alpha_3 - \kappa_1)(\tanh(\lambda_1 d/2) - \lambda_1 d/2)\,. \tag{3.17}$$

These constants allow the solutions for θ, δ, and u, extracted from the solution $\mathbf{x}(z)$, to be written as

$$\theta(z) = 2\beta_1 c_1 \sinh(\lambda_1 z) - 2c_4 \sinh(\lambda_2 z) + f(z) + \frac{az}{2B_1}\,, \tag{3.18}$$

$$\delta(z) = 2c_1 \sinh(\lambda_1 z) + 2c_4 \sinh(\lambda_2 z) + f(z)\,, \tag{3.19}$$

$$u(z) = a\lambda_p \left[\frac{\cosh(\lambda_1 z)}{\cosh(\lambda_1 d/2)} - 1 \right], \tag{3.20}$$

where $f(z)$ is the cubic polynomial

$$f(z) = c_7 z + \frac{az}{12 B_1 K_1^a} \left\{ B_1 \left[6\lambda_p(\eta - \alpha_3 - \kappa_1) + z^2 \right] - 3K_1^a \right\}. \tag{3.21}$$

It can be verified directly that these solutions satisfy (3.1) to (3.3) and the boundary conditions (2.16) and (2.17), in addition to fulfilling the requirement (2.18). It is also evident that there are two length scales that are crucial to the behavior of the above solutions, namely,

$$L_1 = 1/\lambda_1 \quad \text{and} \quad L_2 = 1/\lambda_2\,. \tag{3.22}$$

The length L_1 coincides with the form of the length scale discussed in [11, 9, 3] and [12, p. 418] and is expected to be of the order of a molecular length (or smectic interlayer distance) when the liquid crystal is in the SmA phase far away from the nematic transition temperature. In this context, we also refer the reader to the related experiments and elementary modeling of permeative flow in SmA by Walton, Stewart, and Towler [39]. The length scale L_2 is novel and enters through the presence of the coupling constant B_1. For the typical values listed in Table 1, $L_1 \sim 2.4\,\mathrm{nm}$ and $L_2 \sim 0.25\,\mathrm{nm}$ and so L_1 is expected to be an order of magnitude larger than L_2. This discrepancy could potentially lead to the observation of two distinct boundary layer phenomena. The exact solution for u stated above coincides with that given in [11] and [12, p. 430] for a set of linearized flow equations.

As the SmA phase approaches the nematic (or isotropic) phase, the permeation coefficient λ_p is expected to diverge [12], in the sense that $\lambda_p \to \infty$; in particular, the viscosity coefficients will also vanish as the isotropic phase is approached except for the Newtonian viscosity α_4, in which case $2\eta = \alpha_4$. The equations for θ and δ are irrelevant in the isotropic phase when the characteristic properties of liquid crystals

TABLE 1
Typical material parameters discussed in the text.

Parameter	Typical value
d	10^{-5} m
K_1^n	$5{\times}10^{-12}$ N
K_1^a	$5{\times}10^{-12}$ N
B_0	$8.95{\times}10^{7}$ N m^{-2}
B_1	$4{\times}10^{7}$ N m^{-2}
λ_p	10^{-16} m^2 Pa^{-1} s^{-1}
α_1	-0.0060 Pa s
α_2	-0.0812 Pa s
α_3	-0.0036 Pa s
α_4, τ_1, τ_2	0.0652 Pa s
α_5	0.0640 Pa s
$\kappa_1, \kappa_2, \ldots, \kappa_6$	0.0020 Pa s
$-a$	500 Pa m^{-1}

will be absent, but the solution for u will remain valid in the isotropic limit. It is straightforward to see that taking the appropriate limit as $\lambda_p \to \infty$ in (3.20) leads to

$$u(z) = \frac{a}{2\eta}\left(z^2 - \frac{d^2}{4}\right), \tag{3.23}$$

which is the standard parabolic profile for Poiseuille flow. This particular limiting case has also arisen in an application of linear dynamic theory for SmA when it is assumed that **n** and **a** coincide [12, p. 432].

Illustrative examples of the above exact solutions can now be presented for the typical parameter values stated in Table 1 (cf. [12, 31, 34]). Not all of these selected parameters appear in the linearized equations; nevertheless, they will be required for the asymptotic analysis and the numerical calculation of solutions to the nonlinear equations in the next two sections. A common value for the sample depth has been set at $d = 10\,\mu$m; experimental set-ups of bookshelf aligned samples of SmA commonly have depths that can be varied between $30\,\mu$m and $200\,\mu$m [6] and smectic C samples can have depths from $8\,\mu$m upward [19]. The elastic constants K_1^n and K_1^a and the viscosities α_1 to α_5 are based on representative values for the nematic liquid crystal 5CB [31]. The viscosities τ_1, τ_2 are estimates; κ_1 to κ_6 are expected to be lower in magnitude than the other viscosity coefficients as the SmA phase approaches the nematic phase. The value for B_0 is typical for the smectic layer compression constant [31]. The coupling constant B_1 is in accord with the estimates by Ribotta and Durand [27] ($B_1 \lesssim B_0$) for SmA and the value for the permeation constant λ_p is that estimated by Kléman and Lavrentovich [20, p. 328] (previous measurements for λ_p by Chan and Webb [7] for lamellar bilayers were substantially smaller that this: the value chosen in Table 1 agrees with the experimental evidence reported by Krüger [21], as discussed in [20]). The value for the applied pressure gradient is of the approximate magnitude used experimentally for nematics in [25, 26] when $-a = -p_{,x} \sim \Delta p/L$, where Δp can be of the order 20 Pa and L of the order 35 mm.

The solutions for θ and δ are displayed in Figure 3, where their boundary values have been fixed at $\theta_0 = 0.2\,$rad and $\delta_0 = 0.15\,$rad. Figure 3(a) shows that θ and δ virtually coincide except within regions very close to the boundaries and that their profiles are almost linear across the central bulk of the sample. Although not

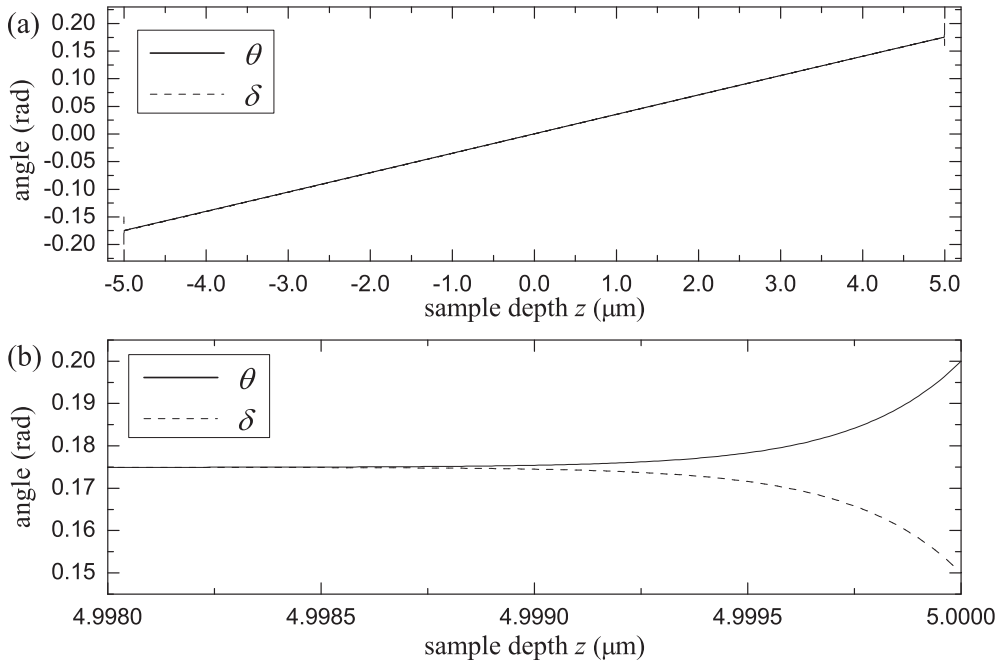

FIG. 3. *Plots of the exact solutions for θ and δ provided by* (3.18) *and* (3.19) *using the material parameter values stated in Table* 1 *when $\theta_0 = 0.2$ rad and $\delta_0 = 0.15$ rad.* (a) *Solutions over the full sample depth $-d/2 \le z \le d/2$. The profile is virtually linear away from the boundaries, as explained in the text.* (b) *The occurrence of a boundary layer is evident near the boundary at $z = d/2$, with a similar effect at $z = -d/2$, by symmetry. The boundary layer is roughly of the order of $L_2 = \sqrt{K_1^a/2B_1} \sim 0.25$ nm.*

represented here, the polynomial $f(z)$ is almost indistinguishable from the orientation angles across the center of the sample and therefore $f(z)$ is a good approximation to θ and δ far from the sample boundaries. Figure 3(b) shows the boundary layer near $z = d/2$. As expected from the above analysis, this boundary layer is approximately of the order of $L_2 = \sqrt{K_1^a/2B_1}$. These results, from the linearized equations, do not exhibit some aspects of the boundary layer behavior that have been reported elsewhere for nonlinear static equations of SmA [32, 36, 13, 14]; the length scale for the boundary layer effect closest to the boundary in the statics of SmA is known [32] to be similarly controlled by a term that is also proportional to $1/\sqrt{B_1}$ (albeit in a different context that does not involve flow). For example, there is a greater interplay between θ and δ near the boundaries which results in novel "competing" preferences in the relative orientations of these angles that are driven by nonlinear contributions to the governing equations (which can also include weak anchoring of the director) and are necessarily absent from the above linear analysis. Such effects were observed to occur over two different length scales in statics: one is clearly similar in form to L_2, but the other cannot be related to L_1 since this length scale, which involves viscosity and permeation, can arise only when flow is present.

Figure 4(a) shows the symmetrical profile of the solution for the velocity u, which is clearly reminiscent of non-Newtonian plug flow. There is a boundary layer effect at each boundary and an example is shown in Figure 4(b) at the $z = d/2$ boundary. The width of the boundary layer, δ^*, may be provided by a standard measure of

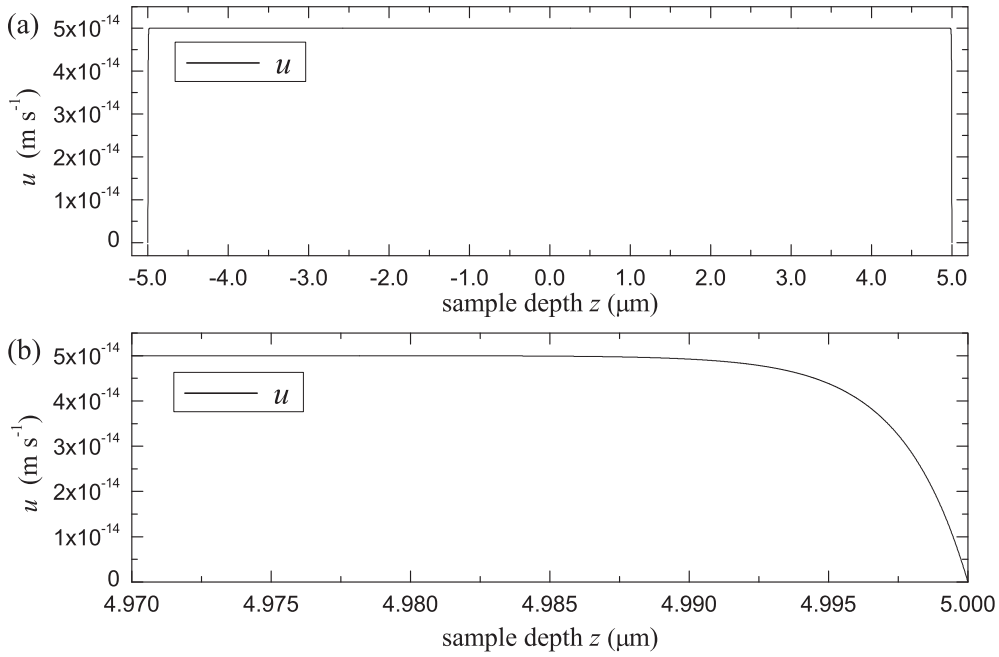

FIG. 4. *Plots of the solution for u given by* (3.20)*, using the material parameters from Table* 1. (a) *The velocity profile for u across the sample $-d/2 \le z \le d/2$.* (b) *The boundary layer near $z = d/2$; a similar effect occurs at $z = -d/2$, by symmetry. The boundary layer can be estimated via* (3.24) *and, in this example, is of the order of $L_1 = \sqrt{\eta\lambda} \sim 2.4\,nm$.*

"displacement thickness" for fluids near boundaries, defined for semi-infinite samples in [4, p. 311]; such a definition is known to generally underestimate the actual boundary layer depth but it does nevertheless provide a rigorous and consistent method of measurement. We find that in this case we may introduce an analogous finite sample depth version as

$$\delta^* = \int_{-\frac{d}{2}}^{0} \left(1 - \frac{u(z)}{u(0)}\right) dz = \frac{1}{4\lambda_1} \operatorname{cosech}^2(\lambda_1 d/4)\,(2\sinh(\lambda_1 d/2) - \lambda_1 d)\,, \tag{3.24}$$

where the usual upper limit of infinity in the integral version for semi-infinite samples has been replaced by zero, where the maximum value of the velocity, $u(0)$, occurs in a finite sample. It turns out that $\delta^* \sim 2.4\,\mathrm{nm}$, which, in this particular example, happens to coincide with $L_1 = \sqrt{\eta\lambda_p}$.

The role of L_2 as a dominant length scale for boundary effects is now evident in the solutions for the orientation angles θ and δ, whereas L_1 appears to control the displacement thickness in the velocity profile of u. Two length scales will also be expected to arise naturally when the nonlinear equations are investigated in the context of boundary layer phenomena.

4. Asymptotic solutions to the nonlinear equations. In this section we will examine asymptotic solutions to the governing nonlinear dynamic equations (2.29), (2.35), and (2.37) subject to the boundary conditions (2.16) and (2.17) and the interior

symmetry requirement (2.18). We begin by noticing that (2.35) may be replaced by the equation

$$\frac{\mathrm{d}\tilde{t}_{13}}{\mathrm{d}z} = a + \frac{u}{\lambda_p} \tag{4.1}$$

by substituting for the derivative of J_3 via (2.37). First, we observe that (2.29), (2.37), and (4.1) are invariant under the transformations

$$u(z) = u(-z), \quad \theta(z) = -\theta(-z), \quad \delta(z) = -\delta(-z). \tag{4.2}$$

Together with the boundary conditions in (2.16), (2.17) and the interior condition (2.18), this might suggest that we can replace the problem formulated for $-d/2 \leq z \leq d/2$ with one formulated on $0 \leq z \leq d/2$ having the boundary conditions

$$\frac{\mathrm{d}u}{\mathrm{d}z} = 0, \quad \theta = 0, \quad \delta = 0, \quad \frac{\mathrm{d}^2\delta}{\mathrm{d}z^2} = 0, \quad \text{at } z = 0, \tag{4.3}$$

$$u = 0, \quad \theta = \theta_0, \quad \delta = \delta_0, \quad \text{at } z = d/2. \tag{4.4}$$

Nevertheless, we will not do this here; see the appendix for a discussion on this matter.

4.1. Nondimensionalization. We choose to rescale by setting

$$z \sim d, \quad u \sim [u], \tag{4.5}$$

where $[u] = -\lambda_p a\,(>0)$, so that (2.29), (2.37), and (4.1) become, respectively,

$$\left\{\cos(\theta-\delta) - \frac{B_0}{B_1}\left[\sec\delta + \cos(\theta-\delta) - 2\right]\right\}\sin(\theta-\delta) - \frac{K_1^n}{B_1 d^2}\cos\theta\frac{\mathrm{d}^2}{\mathrm{d}z^2}\sin\theta$$
$$+ \frac{[u]}{B_1 d}\frac{\mathrm{d}u}{\mathrm{d}z}\left[\alpha_3\cos^2\theta - \alpha_2\sin^2\theta + \kappa_1\cos(\theta+\delta)\right] = 0, \tag{4.6}$$

$$\frac{B_1\lambda_p}{[u]\,d}\frac{\mathrm{d}}{\mathrm{d}z}\Bigg(\cos^2\delta\left[\frac{K_1^a}{B_1 d^2}\cos\delta\frac{\mathrm{d}^2}{\mathrm{d}z^2}\sin\delta + \Bigg(\cos(\theta-\delta) - \frac{B_0}{B_1}\left[\sec\delta + \cos(\theta-\delta) - 2\right]\Bigg)\sin(\theta-\delta)\right]$$
$$- \frac{B_0}{B_1}\sin\delta\left[\sec\delta + \cos(\theta-\delta) - 2\right]\Bigg) + u = 0, \tag{4.7}$$

$$\frac{[u]\,\alpha_4}{d^2}\frac{\mathrm{d}}{\mathrm{d}z}\Bigg(\frac{\mathrm{d}u}{\mathrm{d}z}\Bigg\{\frac{1}{2}\left(1 + \frac{\alpha_5}{\alpha_4} - \frac{\alpha_2}{\alpha_4} + \frac{\tau_2}{\alpha_4}\right) + \frac{1}{4}\left[\frac{\alpha_1}{\alpha_4}\sin^2(2\theta) + \frac{\tau_1}{\alpha_4}\sin^2(2\delta)\right]$$
$$+ \frac{\kappa_1}{\alpha_4}\cos(\theta+\delta) + \frac{\kappa_6}{\alpha_4}\cos(\theta-\delta) + \left(\frac{\alpha_2}{\alpha_4} + \frac{\alpha_3}{\alpha_4}\right)\cos^2\theta$$
$$+ \frac{1}{2}\left[\frac{\kappa_2}{\alpha_4}\sin^2(\theta+\delta) + \frac{\kappa_3}{\alpha_4}\sin(2\theta)\sin(2\delta)\right]$$
$$+ \sin(\theta+\delta)\left[\frac{\kappa_4}{\alpha_4}\sin(2\theta) + \frac{\kappa_5}{\alpha_4}\sin(2\delta)\right]\Bigg\}\Bigg) = a + \frac{[u]}{\lambda_p}u. \tag{4.8}$$

These three equations form the basis for the analysis in this section.

Set

$$B=\frac{B_0}{B_1},\quad \bar\alpha_1=\frac{\alpha_1}{\alpha_4},\quad \bar\alpha_2=\frac{\alpha_2}{\alpha_4},\quad \bar\alpha_3=\frac{\alpha_3}{\alpha_4},\quad \bar\alpha_5=\frac{\alpha_5}{\alpha_4},\quad \bar\tau_1=\frac{\tau_1}{\alpha_4},\quad \bar\tau_2=\frac{\tau_2}{\alpha_4},$$
$$\bar\kappa_1=\frac{\kappa_1}{\alpha_4},\quad \bar\kappa_2=\frac{\kappa_2}{\alpha_4},\quad \bar\kappa_3=\frac{\kappa_3}{\alpha_4},\quad \bar\kappa_4=\frac{\kappa_4}{\alpha_4},\quad \bar\kappa_5=\frac{\kappa_5}{\alpha_4},\quad \bar\kappa_6=\frac{\kappa_6}{\alpha_4},\tag{4.9}$$

where all these are $O(1)$ constants. The parameter B is a measure of the relative influence of the coupling constant B_1 and compression constant B_0; it is known from the analysis of static configurations that a small variation in this control parameter has a high influence on θ and δ within a boundary layer [32]. Equations (4.6) to (4.8) become, respectively,

$$\{\cos(\theta-\delta)-B\left[\sec\delta+\cos(\theta-\delta)-2\right]\}\sin(\theta-\delta)$$
$$-\frac{K_1^n}{B_1d^2}\cos\theta\frac{\mathrm{d}^2}{\mathrm{d}z^2}\sin\theta-\frac{\lambda_p a\alpha_4}{B_1 d}\frac{\mathrm{d}u}{\mathrm{d}z}\left[\bar\alpha_3\cos^2\theta-\bar\alpha_2\sin^2\theta+\bar\kappa_1\cos(\theta+\delta)\right]=0,\tag{4.10}$$

(4.11)

$$\frac{\mathrm{d}}{\mathrm{d}z}\left(\cos^2\delta\left[\frac{K_1^a}{B_1d^2}\cos\delta\frac{\mathrm{d}^2}{\mathrm{d}z^2}\sin\delta+(\cos(\theta-\delta)-B\left[\sec\delta+\cos(\theta-\delta)-2\right])\sin(\theta-\delta)\right]\right.$$
$$\left.-B\sin\delta\left[\sec\delta+\cos(\theta-\delta)-2\right]\right)-\left(\frac{ad}{B_1}\right)u=0,$$

$$-\frac{\lambda_p\alpha_4}{d^2}\frac{\mathrm{d}}{\mathrm{d}z}\left(\frac{\mathrm{d}u}{\mathrm{d}z}\left\{\frac12(1+\bar\alpha_5-\bar\alpha_2+\bar\tau_2)+\frac14\left[\bar\alpha_1\sin^2(2\theta)+\bar\tau_1\sin^2(2\delta)\right]\right.\right.$$
$$+\bar\kappa_1\cos(\theta+\delta)+\bar\kappa_6\cos(\theta-\delta)+(\bar\alpha_2+\bar\alpha_3)\cos^2\theta$$
$$+\frac12\left[\bar\kappa_2\sin^2(\theta+\delta)+\bar\kappa_3\sin(2\theta)\sin(2\delta)\right]$$
$$\left.\left.+\sin(\theta+\delta)\left[\bar\kappa_4\sin(2\theta)+\bar\kappa_5\sin(2\delta)\right]\right\}\right)=1-u.\tag{4.12}$$

From Table 1, we have

$$\frac{\lambda_p\alpha_4}{d^2}\sim10^{-9},\quad \frac{K_1^n}{B_1d^2}\sim10^{-9},\quad \frac{K_1^a}{B_1d^2}\sim10^{-9},\quad \frac{ad}{B_1}\sim10^{-10},\tag{4.13}$$

which suggests that (4.10) to (4.12) will have boundary layers at $z=\pm1/2$ of thickness

$$\left(K_1^n/B_1\right)^{1/2}/d,\quad \left(K_1^a/B_1\right)^{1/2}/d,\quad \left(\lambda_p\alpha_4\right)^{1/2}/d,\tag{4.14}$$

respectively, i.e., of order $\sim10^{-9/2}$.

4.2. The static case. Consider first the case with $u=0$. Denote

$$\varepsilon_a=\frac{K_1^a}{B_1d^2},\quad \varepsilon_n=\frac{K_1^n}{B_1d^2}.\tag{4.15}$$

Since $\varepsilon_a\sim10^{-9},\varepsilon_n\sim10^{-9}$, we choose to set

$$\varepsilon_a=\varepsilon,\quad \varepsilon_n=\beta\varepsilon,\tag{4.16}$$

where β is an $O(1)$ constant; in fact, from the values in Table 1, $\beta=1$. To begin, we first examine the two equations

$$\{\cos(\theta-\delta)-B\left[\sec\delta+\cos(\theta-\delta)-2\right]\}\sin(\theta-\delta)-\beta\varepsilon\cos\theta\frac{\mathrm{d}^2}{\mathrm{d}z^2}\sin\theta=0\tag{4.17}$$

and

(4.18)
$$\frac{\mathrm{d}}{\mathrm{d}z}\Bigg(\cos^2\delta\left[\varepsilon\cos\delta\frac{\mathrm{d}^2}{\mathrm{d}z^2}\sin\delta+(\cos(\theta-\delta)-B\left[\sec\delta+\cos(\theta-\delta)-2\right])\sin(\theta-\delta)\right] \\ -B\sin\delta\left[\sec\delta+\cos(\theta-\delta)-2\right]\Bigg)=0;$$

the second of these implies that

$$\cos^2\delta\left[\varepsilon\cos\delta\frac{\mathrm{d}^2}{\mathrm{d}z^2}\sin\delta+(\cos(\theta-\delta)-B\left[\sec\delta+\cos(\theta-\delta)-2\right])\sin(\theta-\delta)\right] \\ -B\sin\delta\left[\sec\delta+\cos(\theta-\delta)-2\right]=C, \tag{4.19}$$

where C is a constant that needs to be determined. In the bulk, (4.17) reduces to

$$\left\{\cos(\theta-\delta)-B\left[\sec\delta+\cos(\theta-\delta)-2\right]\right\}\sin(\theta-\delta)=0, \tag{4.20}$$

which implies that either

$$\cos(\theta-\delta)-B\left[\sec\delta+\cos(\theta-\delta)-2\right]=0 \qquad \text{or} \qquad \sin(\theta-\delta)=0. \tag{4.21}$$

Since the full numerical results indicate that $\theta\approx\delta$, we consider the second possibility. Equation (4.19) then implies that

$$-B\sin\delta\left[\sec\delta-1\right]=C. \tag{4.22}$$

The numerics also indicate that $\delta\ll 1$, which would then imply that $C\ll 1$. There is, however, a slight problem: the "small" term

(4.23)
$$\cos^2\delta\left[\varepsilon\cos\delta\frac{\mathrm{d}^2}{\mathrm{d}z^2}(\sin\delta)+(\cos(\theta-\delta)-B\left[\sec\delta+\cos(\theta-\delta)-2\right])\sin(\theta-\delta)\right]$$

was neglected in (4.19), but all that was left were terms which are themselves "small"; in order to keep track of the size of what is being retained or neglected, formal asymptotic expansions for δ and θ are therefore required.

A consistent formulation turns out to be possible if we have $\theta\sim\varepsilon^{1/2}$; thus, we set

$$\theta=\varepsilon^{1/2}\left(\Theta_0+\varepsilon\Theta_1+\cdots\right), \quad \delta=\varepsilon^{1/2}\left(\Delta_0+\varepsilon\Delta_1+\cdots\right). \tag{4.24}$$

At leading order, $\varepsilon^{1/2}$, (4.17) gives

$$\Theta_0=\Delta_0, \tag{4.25}$$

and, using (4.25), at $\varepsilon^{3/2}$

$$\Theta_1-\Delta_1-\beta\frac{\mathrm{d}^2\Theta_0}{\mathrm{d}z^2}=0. \tag{4.26}$$

At leading order, $\varepsilon^{3/2}$, (4.19) gives, on using (4.25),

$$\frac{\mathrm{d}^2\Delta_0}{\mathrm{d}z^2}+\Theta_1-\Delta_1-\frac{1}{2}B\Delta_0^3=\bar{C}, \tag{4.27}$$

where we have now set $C = \bar{C}\varepsilon^{3/2}$, where $\bar{C} \sim O(1)$, since the constant C must be of order $\varepsilon^{3/2}$. Combining (4.25) to (4.27), we have

$$(1+\beta)\frac{\mathrm{d}^2\Theta_0}{\mathrm{d}z^2} - \frac{1}{2}B\Theta_0^3 = \bar{C}. \tag{4.28}$$

We will need boundary layers near $z = \pm 1/2$. Considering first the boundary layer at $z = 1/2$, we set $z = 1/2 - \varepsilon^{1/2}Z$; (4.17) and (4.18) reduce to just

$$\{\cos(\theta-\delta) - B[\sec\delta + \cos(\theta-\delta) - 2]\}\sin(\theta-\delta) - \beta\cos\theta\frac{\mathrm{d}^2}{\mathrm{d}Z^2}(\sin\theta) = 0, \tag{4.29}$$

$$\cos^2\delta\left[\cos\delta\frac{\mathrm{d}^2}{\mathrm{d}Z^2}(\sin\delta) + (\cos(\theta-\delta) - B[\sec\delta + \cos(\theta-\delta) - 2])\sin(\theta-\delta)\right] - B\sin\delta[\sec\delta + \cos(\theta-\delta) - 2] = C, \tag{4.30}$$

respectively. In this layer, θ, δ are $O(1)$, but we need to consider how to match them to the bulk flow, i.e., as $Z \to \infty$. Since $\theta, \delta \sim \varepsilon^{1/2}$ in the bulk, we might be tempted just to set

$$\theta, \delta \to 0 \quad \text{as } Z \to \infty; \tag{4.31}$$

however, we should first consider the behavior of Θ_0, Δ_0 as $z \to 1/2$.

Returning to (4.28), consider the possibility that

$$(1+\beta)\frac{\mathrm{d}^2\Theta_0}{\mathrm{d}z^2} \sim \frac{1}{2}B\Theta_0^3 \quad \text{when } \frac{1}{2} - z \ll 1. \tag{4.32}$$

This would imply that

$$\Theta_0 \sim \frac{A}{1/2 - z}, \tag{4.33}$$

where A satisfies

$$A\left(4(1+\beta) - BA^2\right) = 0\,; \tag{4.34}$$

the appropriate root for A, which is consistent with the boundary conditions for θ and δ in (2.17), is then

$$A = \left(\frac{4(1+\beta)}{B}\right)^{1/2}. \tag{4.35}$$

Notice also that the form obtained in (4.33) is consistent with the leading-order balance that was assumed in going from (4.28) to (4.32). Next, for the purposes of matching the bulk to the boundary layer flow, we write the bulk solution in terms of the boundary layer variables; thus, at leading order, we have

$$\theta = \varepsilon^{1/2}\Theta_0 = \frac{A}{Z}. \tag{4.36}$$

Hence, we obtain an improvement on (4.31): we now have $\theta, \delta \sim A/Z$ as $Z \to \infty$. Furthermore, in view of this behavior, we observe that (4.30), considered in the

limit as $Z \to \infty$, implies that $C = 0$. In turn, this implies that $\bar{C} = 0$; moreover, the fact that $\mathrm{d}^2\delta/\mathrm{d}z^2 = 0$ at $z = 0$ implies that $\mathrm{d}^2\Theta_0/\mathrm{d}z^2 = 0$ at $z = 0$, and hence that $\Theta_0(0) = 0$. With this result, we have shown that, at this order, the solution in θ is antisymmetric, in the manner discussed at the beginning of section 4.

At this stage, the leading-order problem is still not entirely solved, since we have yet to determine the bulk solution completely. Integrating (4.28), we have

$$\frac{1}{2}(1+\beta)\left(\frac{\mathrm{d}\Theta_0}{\mathrm{d}z}\right)^2 - \frac{1}{8}B\Theta_0^4 = D \tag{4.37}$$

subject to

$$\Theta_0(0) = 0 \tag{4.38}$$

with D a constant to be determined; in addition, (4.33) must be satisfied. It is evident that this must be solved numerically, although solving it as an initial-value problem by starting at $z = 0$ will fail, because the singular behavior at $z = 1/2$ will not be resolved; instead, it is necessary to start at $z = 1/2$ and integrate back to $z = 0$, with D being iterated for, so as to ensure that (4.38) is satisfied. Setting $z = 1/2 - \zeta$, we have

$$\frac{1}{2}(1+\beta)\left(\frac{\mathrm{d}\Theta_0}{\mathrm{d}\zeta}\right)^2 - \frac{1}{8}B\Theta_0^4 = D \tag{4.39}$$

with

$$\Theta_0(1/2) = 0 \quad \text{and} \quad \Theta_0 \sim \frac{A}{\zeta} \quad \text{as } \zeta \to 0. \tag{4.40}$$

Next, set $\Theta_0 = F/\zeta$ so that

$$\frac{1}{2}(1+\beta)\left(\zeta\frac{\mathrm{d}F}{\mathrm{d}\zeta} - F\right)^2 - \frac{1}{8}BF^4 = D\zeta^4. \tag{4.41}$$

Then

$$\zeta\frac{\mathrm{d}F}{\mathrm{d}\zeta} = F \pm \left(\frac{BF^4 + 8D\zeta^4}{4(1+\beta)}\right)^{1/2} \tag{4.42}$$

with

$$F(0) = A \quad \text{and} \quad F(1/2) = 0. \tag{4.43}$$

It is clear that we should take the negative sign in (4.42) in order to ensure that the first requirement in (4.43) is satisfied. The function F is then solved numerically and, after iterating for D, is displayed in Figure 5(a); the constant D was found to be $D \approx 680$. The profile of Θ_0 versus z is shown in Figure 5(b).

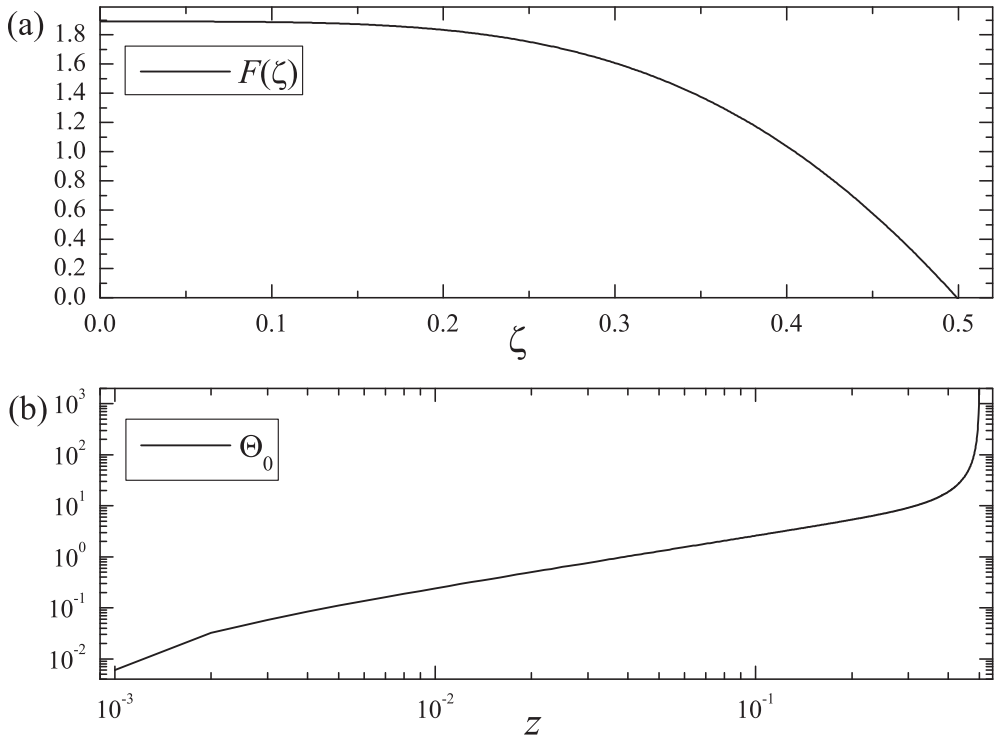

FIG. 5. (a) *The dependence of F upon ζ.* (b) *Θ_0 as a function of z (static case).*

All that remains is to solve the boundary layer equations; to summarize (after all the simplifications) these satisfy

$$\{\cos(\theta-\delta) - B[\sec\delta + \cos(\theta-\delta) - 2]\}\sin(\theta-\delta) - \beta\cos\theta\frac{\mathrm{d}^2}{\mathrm{d}Z^2}(\sin\theta) = 0, \tag{4.44}$$

$$\cos^2\delta\left[\cos\delta\frac{\mathrm{d}^2}{\mathrm{d}Z^2}(\sin\delta) + (\cos(\theta-\delta) - B[\sec\delta + \cos(\theta-\delta) - 2])\sin(\theta-\delta)\right] - B\sin\delta[\sec\delta + \cos(\theta-\delta) - 2] = 0, \tag{4.45}$$

since $C \equiv 0$ has been established, subject to

$$\theta = \theta_0, \quad \delta = \delta_0, \quad \text{at } Z = 0 \quad \text{with} \quad \theta, \delta \sim \frac{A}{Z} \quad \text{as } Z \to \infty. \tag{4.46}$$

The numerical solutions (computed with COMSOL Multiphysics) for δ and θ are shown in Figure 6; the boundary values have been selected as $\theta_0 = \pi/6$ and $\delta_0 = \pi/16$, these being close to physically realistic data. Figure 6(a) shows the slow algebraic decay of θ and δ, which is why such a large value of Z_∞, the location of the outer edge of the computational domain, is required. Figure 6(b) shows θ and δ closer to $Z = 0$; the characteristic hump in δ is visible.

4.3. The dynamic case. We now consider what happens when $u \neq 0$. Setting

$$\gamma = -ad/B_1, \quad \nu = \frac{\lambda_p\alpha_4}{d^2}, \tag{4.47}$$

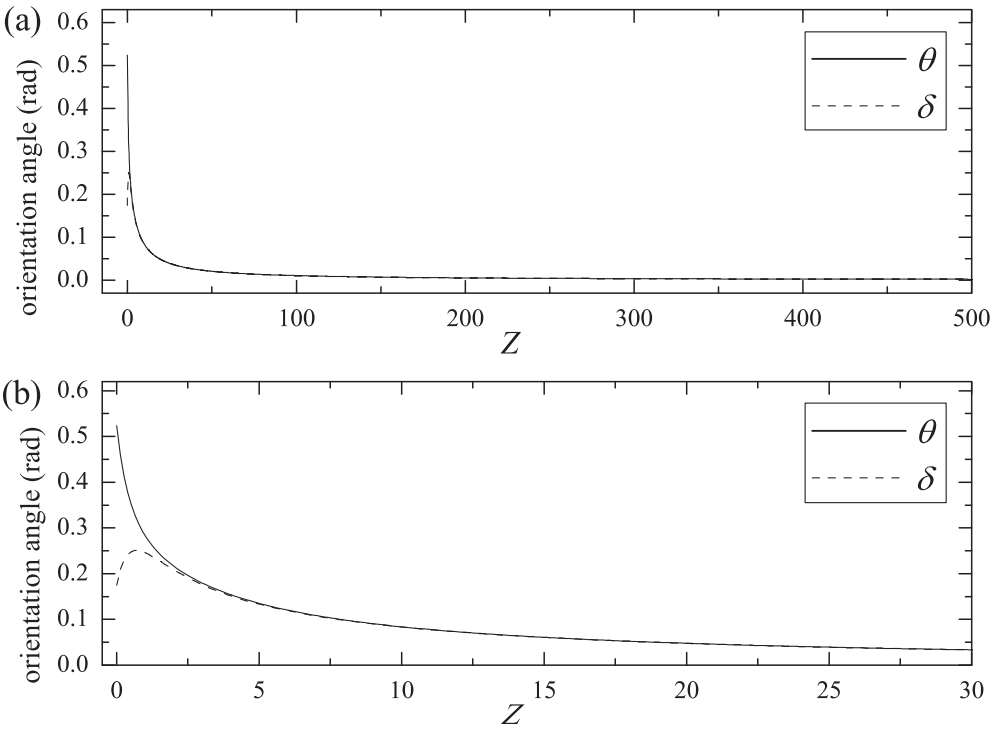

FIG. 6. *The dependence of θ and δ upon Z (static case).* (a) *The domain* $0 \leq Z \leq 500$. (b) *A restriction of the result in* (a) *to the domain* $0 \leq Z \leq 30$, *which emphasizes the boundary layer effects.*

where $\gamma, \nu \ll 1$, we have

$$\{\cos(\theta-\delta) - B[\sec\delta + \cos(\theta-\delta) - 2]\}\sin(\theta-\delta) - \beta\varepsilon\cos\theta\frac{\mathrm{d}^2}{\mathrm{d}z^2}\sin\theta + \gamma\nu\frac{\mathrm{d}u}{\mathrm{d}z}\left[\bar{\alpha}_3\cos^2\theta - \bar{\alpha}_2\sin^2\theta + \bar{\kappa}_1\cos(\theta+\delta)\right] = 0, \tag{4.48}$$

$$\frac{\mathrm{d}}{\mathrm{d}z}\Bigg(\cos^2\delta\left[\varepsilon\cos\delta\frac{\mathrm{d}^2}{\mathrm{d}z^2}\sin\delta + (\cos(\theta-\delta) - B[\sec\delta + \cos(\theta-\delta) - 2])\sin(\theta-\delta)\right] - B\sin\delta[\sec\delta + \cos(\theta-\delta) - 2]\Bigg) = -\gamma u, \tag{4.49}$$

$$-\nu\frac{\mathrm{d}}{\mathrm{d}z}\Bigg(\frac{\mathrm{d}u}{\mathrm{d}z}\Bigg\{\frac{1}{2}(1 + \bar{\alpha}_5 - \bar{\alpha}_2 + \bar{\tau}_2) + \frac{1}{4}\left[\bar{\alpha}_1\sin^2(2\theta) + \bar{\tau}_1\sin^2(2\delta)\right] + \bar{\kappa}_1\cos(\theta+\delta) + \bar{\kappa}_6\cos(\theta-\delta) + (\bar{\alpha}_2 + \bar{\alpha}_3)\cos^2\theta + \frac{1}{2}\left[\bar{\kappa}_2\sin^2(\theta+\delta) + \bar{\kappa}_3\sin(2\theta)\sin(2\delta)\right] + \sin(\theta+\delta)\left[\bar{\kappa}_4\sin(2\theta) + \bar{\kappa}_5\sin(2\delta)\right]\Bigg\}\Bigg) = 1 - u. \tag{4.50}$$

In order to proceed with an asymptotic analysis, it transpires that it will be useful to split the analysis over four regimes, labeled I to IV in a natural ordering, as

indicated schematically in Figure 9 later. It proves expedient, for calculations in the following subsections, to consider region III first, followed sequentially by regions IV, II, and I.

4.3.1. In the bulk (bulk region III). Consider the leading-order balance of terms for (4.48) to (4.50) in the bulk. Equation (4.50) implies that $u \approx 1$. Noting that ε, γ, ν are more or less the same order of magnitude, i.e., $10^{-9} - 10^{-10}$, the leading-order balance for (4.48) gives the same result as did (4.17), i.e., $\theta \approx \delta$. The major difference between the static and dynamic cases arises in (4.49). Suppose that $\delta \sim O([\delta])$, where $[\delta]$ is to be determined, although clearly $[\delta] \ll 1$. Equation (4.49) has terms with magnitudes

$$\varepsilon\,[\delta]\,, \quad [\delta]^3\,, \quad \gamma\,. \tag{4.51}$$

Consider, in turn, the possible leading-order balances in (4.49):

1. The balance used for the static case, $[\delta] \sim \varepsilon^{1/2}$, is no longer valid here, since $\varepsilon^{3/2} \ll \gamma$.
2. We cannot have $\varepsilon[\delta] \sim \gamma$ since $\gamma/\varepsilon \sim O(1)$, whereas we must have $[\delta] \ll 1$.
3. The only remaining possibility is $[\delta]^3 \sim \gamma$, which implies $[\delta] \sim \gamma^{1/3}$. This is feasible since $\varepsilon \ll \gamma^{2/3}$.

By setting

$$\theta = \gamma^{1/3}\left(\Theta_0 + \gamma^{1/3}\Theta_1 + \cdots\right), \quad \delta = \gamma^{1/3}\left(\Delta_0 + \gamma^{1/3}\Delta_1 + \cdots\right), \tag{4.52}$$

(4.48) gives, at leading order, $O(\gamma^{1/3})$ and $\Theta_0 - \Delta_0 = 0$. Equation (4.49) gives, at leading order, $O(\gamma)$, noting that $\varepsilon\gamma^{1/3} \ll \gamma$,

$$\frac{\mathrm{d}}{\mathrm{d}z}\left(\frac{1}{2}B\Theta_0^3\right) = 1, \tag{4.53}$$

whence

$$\Theta_0 = \Delta_0 = \left(\frac{2z + A_+^*}{B}\right)^{1/3}, \tag{4.54}$$

where A_+^* is a constant to be determined. For $z < 0$, there is something similar, namely,

$$\Theta_0 = \Delta_0 = \left(\frac{2z + A_-^*}{B}\right)^{1/3}. \tag{4.55}$$

4.3.2. Boundary layer at $z = 0$ (bulk region IV). However, it is evident that Δ_0 will not satisfy the boundary condition at $\Delta_0''(0) = 0$, and so we need a boundary layer there. Suppose it is of thickness $[z]$. We set

$$z = [z]\,Z, \quad \Theta_0 = [\Theta_0]\,\bar{\Theta}_0, \quad \Delta_0 = [\Delta_0]\,\bar{\Delta}_0, \tag{4.56}$$

where $[z]\,, [\Theta_0]$, and $[\Delta_0]$ are scales to be determined, although we expect

$$[z]\,, \quad [\Theta_0]\,, \quad [\Delta_0] \ll 1. \tag{4.57}$$

Assume for the moment that the leading-order balance in (4.48) leads to

$$\{\cos(\theta - \delta) - B\,[\sec\delta + \cos(\theta - \delta) - 2]\}\sin(\theta - \delta) = 0\,, \tag{4.58}$$

which implies that $[\Theta_0] = [\Delta_0]$ and

$$\bar{\Theta}_0 = \bar{\Delta}_0. \tag{4.59}$$

Furthermore, from (4.49),

$$\frac{1}{[z]}\frac{\mathrm{d}}{\mathrm{d}Z}\left(-\frac{\varepsilon\gamma^{1/3}[\Delta_0]}{[z]^2}\frac{\mathrm{d}^2\bar{\Delta}_0}{\mathrm{d}Z^2} + \frac{\gamma[\Delta_0]^3}{2}B\bar{\Delta}_0^3\right) = \gamma\,. \tag{4.60}$$

Thus, to retain all terms in (4.60), we need

$$\frac{\varepsilon\gamma^{1/3}[\Delta_0]}{[z]^2} = \gamma[z] = \gamma[\Delta_0]^3\,, \tag{4.61}$$

and hence

$$[z] = \varepsilon^{3/8}\gamma^{-1/4}, \quad [\Delta_0] \sim \varepsilon^{1/8}\gamma^{-1/12} \tag{4.62}$$

(and consequently $\theta, \delta \sim \gamma^{1/3}[\Delta_0] = \gamma^{1/3}[\Theta_0]$, i.e., $\theta, \delta \sim \epsilon^{1/8}\gamma^{1/4}$). We are therefore left with

$$\frac{\mathrm{d}}{\mathrm{d}Z}\left(-\frac{\mathrm{d}^2\bar{\Delta}_0}{\mathrm{d}Z^2} + \frac{1}{2}B\bar{\Delta}_0^3\right) = 1, \tag{4.63}$$

and so

$$-\frac{\mathrm{d}^2\bar{\Delta}_0}{\mathrm{d}Z^2} + \frac{1}{2}B\bar{\Delta}_0^3 = Z + A, \tag{4.64}$$

where A is a constant to be determined. For correct matching as $Z \to \pm\infty$, we need $A_\pm^* = 0$. To see this we first observe from (4.64) that $\bar{\Delta}_0 \sim (2Z/B)^{1/3}$ when $Z \gg 1$. However,

$$\Delta_0 = [\Delta_0]\bar{\Delta}_0 = [\Delta_0]\left(\frac{2[z]z}{B}\right)^{1/3} = \left(\frac{2Z}{B}\right)^{1/3}, \tag{4.65}$$

and so we deduce that $A_\pm^* = 0$.

Equation (4.64) now remains, subject to the requirements

$$\frac{\mathrm{d}^2\bar{\Delta}_0}{\mathrm{d}Z^2} = 0 \quad \text{at } Z = 0\,, \quad \text{and} \quad \bar{\Delta}_0 \sim \left(\frac{2Z}{B}\right)^{1/3} \quad \text{as } Z \to \pm\infty\,, \tag{4.66}$$

which can be solved numerically. Figure 7(a) shows $\bar{\Delta}_0$ versus Z for $A = -1, 0, 1$ and Figure 7(b) shows $\bar{\Delta}_0''(0)$ versus A; clearly, the requirement that $\bar{\Delta}_0''(0) = 0$ necessitates that $A = 0$.

However, we should check that the assumption that led to (4.54) was correct. For this, we require that

$$\gamma^{1/3}[\Theta_0] \gg \frac{\varepsilon\gamma^{1/3}[\Theta_0]}{[z]^2}, \tag{4.67}$$

which reduces, on using (4.59) and (4.62), to $\gamma^{-1/2} \gg \varepsilon^{1/4}$, which is easily satisfied.

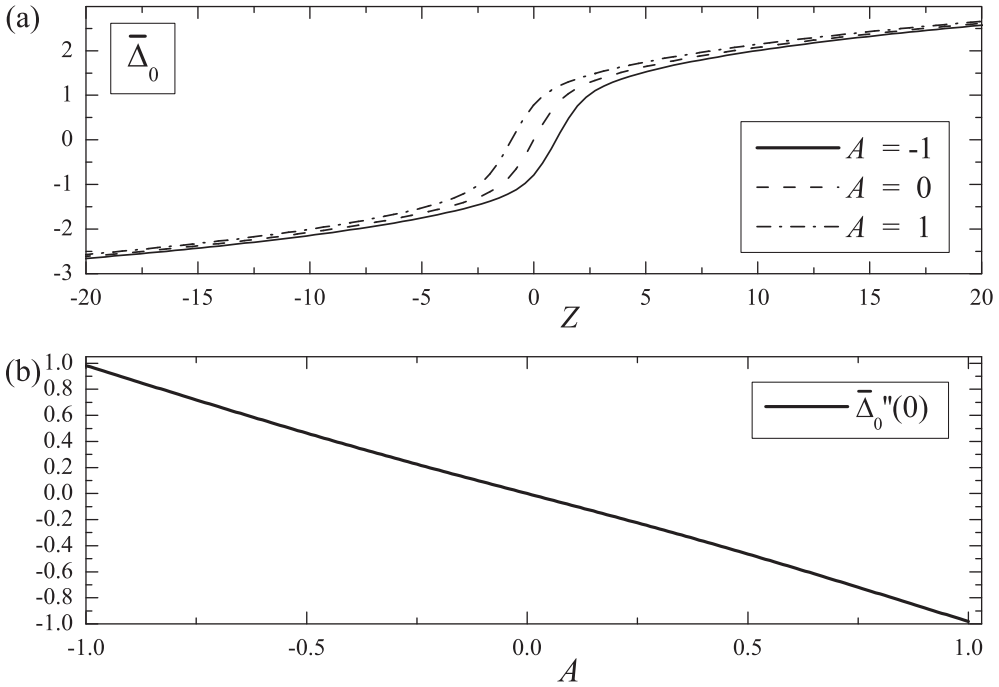

FIG. 7. (a) *The dependence of* $\bar{\Delta}_0$ *upon* Z *for* $A = -1$, 0, *and* 1. (b) *The dependence of* $\bar{\Delta}_0''(0)$ *upon* A.

4.3.3. Transition layer (secondary boundary layer II). Again, we will need boundary layers near $z = \pm 1/2$. First, we will need $\theta, \delta \sim \gamma^{1/3}$, so as to be able to match to the bulk. Set $z = \frac{1}{2} - [z]\zeta$. The orders of magnitude of the relevant terms in (4.49) are

$$\frac{\varepsilon\gamma^{1/3}}{[z]^3}, \quad \frac{\gamma^{2/3}}{[z]}, \quad \frac{\gamma}{[z]}, \quad \gamma\,. \tag{4.68}$$

This time, not all terms can be accommodated, since $[z] \ll 1$, so the leading-order balance must be between the first and the third term; thus,

$$\frac{\varepsilon\gamma^{1/3}}{[z]^3} \sim \frac{\gamma}{[z]} \Longrightarrow [z] = \varepsilon^{1/2}\gamma^{-1/3}. \tag{4.69}$$

Setting

$$z = \frac{1}{2} - \varepsilon^{1/2}\gamma^{-1/3}\zeta, \quad \delta = \gamma^{1/3}\Delta, \quad \theta = \gamma^{1/3}\Theta, \tag{4.70}$$

(4.48) and (4.49) give, at leading order,

$$\Delta = \Theta, \tag{4.71}$$

$$\frac{\mathrm{d}}{\mathrm{d}\zeta}\left(\frac{\mathrm{d}^2\Delta}{\mathrm{d}\zeta^2} - \frac{1}{2}B\Delta^3\right) = 0, \tag{4.72}$$

respectively, with

$$\Delta \to \left(\frac{1}{B}\right)^{1/3} \quad \text{as } \zeta \to \infty. \tag{4.73}$$

Note that as $\zeta \to \infty, \Delta$ must tend to Δ_0 in the bulk (given by (4.58)) as $z \to \frac{1}{2}$.

Note incidentally that the first term and last terms on the left-hand side of (4.48) are of order $\gamma^{1/3}$ and $\gamma^{2/3}\varepsilon^{-1/2}\nu$, respectively. However, since ε and ν are of the same order of magnitude in this problem, we use the fact that $\varepsilon^{3/2} \ll \gamma$ to conclude that $\gamma^{1/3} \gg \gamma^{4/3}\varepsilon^{-1/2}\nu$, which then leads to (4.71). Also, observe that the terms that have been retained in (4.72) from the original equation (4.49) are of order $\gamma^{4/3}\varepsilon^{-1/2}$, whereas the term on the right-hand side of (4.49) is of order γ. Again, we use $\varepsilon^{3/2} \ll \gamma$ to see that $\gamma^{4/3}\varepsilon^{-1/2} \gg \gamma$.

Equations (4.72) and (4.73) then lead to

$$\frac{\mathrm{d}^2\Delta}{\mathrm{d}\zeta^2} - \frac{1}{2}B\Delta^3 = -\frac{1}{2}. \tag{4.74}$$

Observe the similarity between (4.74) and (4.32) in the "static" case; in particular, we can note that, for $\zeta \ll 1$, $\Delta \sim A/\zeta$ with $A(2 - \frac{1}{2}BA^2) = 0$. Selecting the positive root then implies that

$$\Delta \sim \left(\frac{4}{B}\right)^{1/2} \frac{1}{\zeta}. \tag{4.75}$$

Now, we have, on multiplying (4.74) by $\mathrm{d}\Delta/\mathrm{d}\zeta$, integrating, and using (4.73),

$$\frac{1}{2}\left(\frac{\mathrm{d}\Delta}{\mathrm{d}\zeta}\right)^2 - \frac{1}{8}B\Delta^4 = -\frac{1}{2}\Delta + \frac{3}{8}\left(\frac{1}{B}\right)^{1/3}. \tag{4.76}$$

To solve (4.76) numerically, set $\Delta = G/\zeta$ so that

$$\zeta\frac{\mathrm{d}G}{\mathrm{d}\zeta} = G - \sqrt{\frac{1}{4}BG^4 - \zeta^3 G + \frac{3}{4}\left(\frac{1}{B}\right)^{1/3}\zeta^4}, \tag{4.77}$$

again selecting the positive root, subject to $G(0) = (4/B)^{1/2}$. Solving for G numerically, we obtain the profile for Δ as shown in Figure 8, which also shows the function G. Observe also that since $\nu \ll \left(\varepsilon^{1/2}\gamma^{-1/3}\right)^2$, (4.50) simply reduces to $u = 1$ in this layer, as in the two bulk regions.

4.3.4. Boundary layer at $z = \frac{1}{2}$ (primary boundary layer I). However, Δ (and Θ) as determined above still cannot satisfy the boundary conditions at $z = 1/2$. For this, we need a sublayer where $\theta, \delta \sim O(1)$ and $\frac{1}{2} - z \sim \varepsilon^{1/2}$; setting $z = 1/2 - \varepsilon^{1/2}Z$, (4.48) and (4.49) reduce, at leading order, to just

$$\{\cos(\theta - \delta) - B[\sec\delta + \cos(\theta - \delta) - 2]\}\sin(\theta - \delta) - \beta\cos\theta\frac{\mathrm{d}^2}{\mathrm{d}Z^2}\sin\theta = 0, \tag{4.78}$$

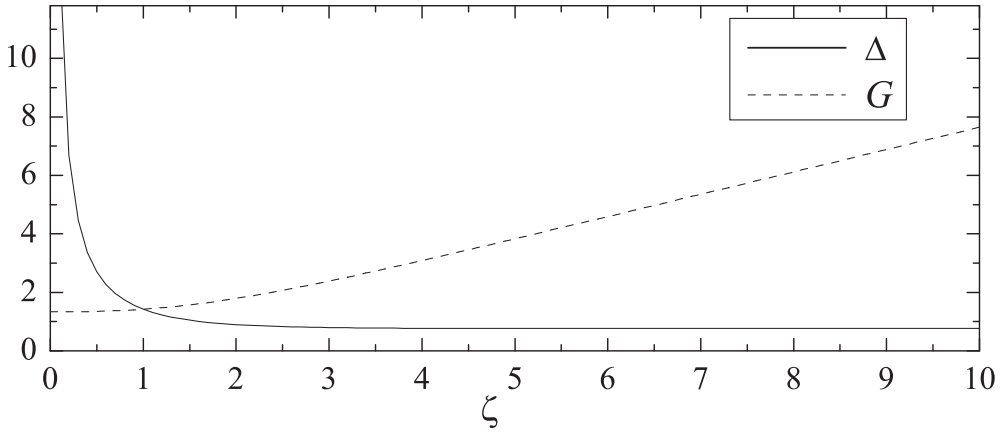

FIG. 8. *The dependence of* Δ *and* G *on* ζ.

$$\cos^2\delta\left[\cos\delta\frac{\mathrm{d}^2}{\mathrm{d}Z^2}\sin\delta+(\cos(\theta-\delta)-B[\sec\delta+\cos(\theta-\delta)-2])\sin(\theta-\delta)\right] - B\sin\delta[\sec\delta+\cos(\theta-\delta)-2]=C^*, \tag{4.79}$$

where C^* is a constant to be determined. In a similar fashion to the analysis of the static case (cf. (4.17) to (4.35)) we note that

$$\theta,\delta\sim\left(\frac{4}{B}\right)^{1/2}\frac{1}{Z} \tag{4.80}$$

and therefore observe that (4.79), considered in the limit as $Z\to\infty$, implies $C^*=0$.

Now, on matching to the layer outside this one, i.e., where $\frac{1}{2}-z\sim\varepsilon^{1/2}\gamma^{-1/3}$, we must have $\theta,\delta\to 0$ as $Z\to\infty$. Note that these equations are almost exactly the same as those for the boundary layer in the "static" case; the only difference is the constant of proportionality, A, for θ,δ as $Z\to\infty$:

$$A=\begin{cases}(4(1+\beta)/B)^{1/2} & \text{"static,"}\\ (4/B)^{1/2} & \text{"dynamic."}\end{cases} \tag{4.81}$$

Thus for the sublayer $\frac{1}{2}-z\sim\varepsilon^{1/2}$ we require to solve numerically (4.78) and (4.79) (with $C^*=0$) subject to the boundary conditions

$$\theta=\theta_0,\ \delta=\delta_0 \quad\text{at}\quad Z=0 \quad\text{with}\quad \theta,\delta\to 0 \quad\text{as}\quad Z\to\infty. \tag{4.82}$$

Note also that the problem for u in this layer, i.e.,

$$\begin{aligned}-\frac{\nu}{\varepsilon}\frac{\mathrm{d}}{\mathrm{d}Z}\Bigg(\frac{\mathrm{d}u}{\mathrm{d}Z}\Bigg\{&\frac{1}{2}(1+\bar\alpha_5-\bar\alpha_2+\bar\tau_2)+\frac{1}{4}\left[\bar\alpha_1\sin^2(2\theta)+\bar\tau_1\sin^2(2\delta)\right]\\ &+\bar\kappa_1\cos(\theta+\delta)+\bar\kappa_6\cos(\theta-\delta)+(\bar\alpha_2+\bar\alpha_3)\cos^2\theta\\ &+\frac{1}{2}\left[\bar\kappa_2\sin^2(\theta+\delta)+\bar\kappa_3\sin(2\theta)\sin(2\delta)\right]\\ &+\sin(\theta+\delta)\left[\bar\kappa_4\sin(2\theta)+\bar\kappa_5\sin(2\delta)\right]\Bigg\}\Bigg)=1-u\end{aligned} \tag{4.83}$$

subject to

$$u = 0 \quad \text{at } Z = 0 \quad \text{with} \quad u \to 1 \quad \text{as } Z \to \infty\,, \tag{4.84}$$

can be solved numerically after we have solved for θ and δ.

4.4. Summary. The asymptotic results from the previous subsections can be summarized as follows. The static problem is characterized by

- a boundary layer where

$$1/2 - z \sim \varepsilon^{1/2}, \quad \theta, \delta \sim 1;$$

- a bulk region where

$$z \ll \frac{1}{2} - \varepsilon^{1/2}, \quad \theta, \delta \sim \varepsilon^{1/2}.$$

The dynamic problem has four key regions of behavior characterized by

- a primary boundary layer (I) where

$$\frac{1}{2} - z \sim \varepsilon^{1/2}, \quad \theta, \delta \sim 1;$$

- a secondary boundary layer and transitional region (II) with

$$\frac{1}{2} - z \sim \varepsilon^{1/2}\gamma^{-1/3}, \quad \frac{1}{2} - z \gg \varepsilon^{1/2}, \quad \theta, \delta \sim \gamma^{1/3};$$

- a bulk region (III) where

$$z \gg \varepsilon^{3/8}\gamma^{-1/4}, \quad \frac{1}{2} - z \gg \varepsilon^{1/2}\gamma^{-1/3}, \quad \theta, \delta \sim \gamma^{1/3};$$

- a bulk region (IV) where

$$z \sim \varepsilon^{3/8}\gamma^{-1/4}, \quad \theta, \delta \sim \varepsilon^{1/8}\gamma^{1/4}.$$

The identification of the behavior of the orientation angles in these four key regions for the dynamic problem is displayed schematically in Figure 9.

5. Comparison with numerical solutions. Figure 10 shows comparisons between the asymptotic results and the numerically derived results for the nonlinear dynamic problem for the fixed parameter values of $\kappa = 1$ and $B = 1$, the other parameters being set to the values indicated in Table 1. For clarity of exposition, the results have been displayed on log-log plots. The left column of plots displays the asymptotically derived results from the previous section for the orientation angles θ and δ and the velocity profile u over the four key layer regions, as indicated. The right column shows the numerically derived solutions to the fully nonlinear dynamic problem. It can be clearly seen that the approximated asymptotic results accurately reflect the behavior of the numerical solutions.

Numerically derived solutions for θ and δ are given in Figure 11. Examples are shown for four sets of values of the key parameter values κ and B, as indicated in the figure. There are clearly significant nonlinear effects in the solutions near the boundary as κ and B vary. The orientation angles close to the boundary, $z \sim 1/2$, over region (I), appear to be particularly sensitive to changes in the values of these control

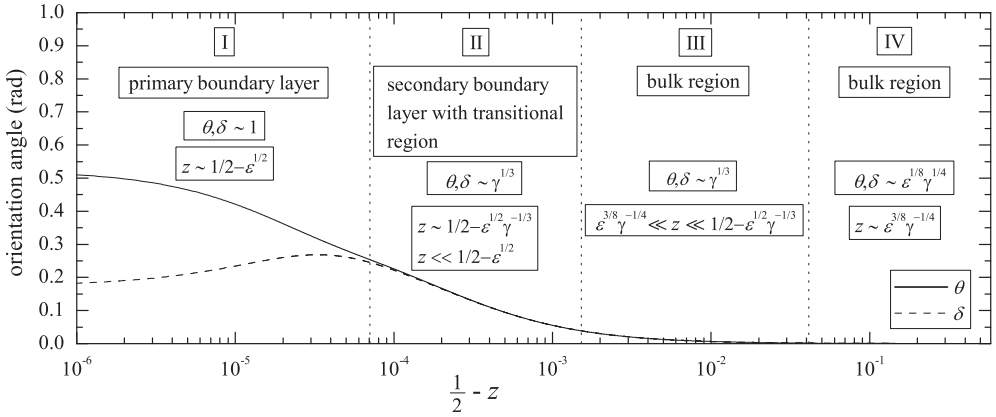

FIG. 9. *A schematic description of the four key regions (separated by dotted vertical lines) that identify the main boundary layer phenomena of the dynamic problem discussed in the text.*

parameters. Similar results were found in the static case in [32]. As an example, we have taken the situation in Figure 11(d) and compared these results for the dynamic problem with those previously derived in Figure 10(d) in [32] for the analogous static problem; in both cases $\kappa = 0.1$ and $B = 0.1$. The comparisons for θ and δ are shown in Figures 12(a) and (b), respectively. Notice that, for emphasis, the vertical axes on these plots are on a log scale in order to highlight the differences between the dynamic and static solutions to this problem. It is clear that flow has a more dramatic effect on the orientation angles close to the central bulk of the sample, corresponding to regions (III) and (IV) in Figure 9, rather than the regions close to the boundaries.

Usually, we would expect agreement between asymptotic and numerical results to improve as the numerical value of an asymptotic parameter tends to its limiting value. For the dynamic case, however, we have a problem. The analysis was for the situation as $\gamma \to 0$; however, if γ becomes too small $\left(\gamma \sim \varepsilon^{3/2}\right)$, we will simply recover the static case. Thus, we should only expect agreement if $\varepsilon^{3/2} \ll \gamma \ll 1$. With $\varepsilon \sim 10^{-9}$ and $\gamma \sim 10^{-10}$, this condition is satisfied; however, decreasing γ (by decreasing -a) may lead to a result that we were not expecting. Paradoxically, in order to obtain good agreement between asymptotic and numerical results to see the trend it is necessary to choose $a = -50000, -5000, -500$, rather than $-500, -50, -5$.

6. Discussion. This article has investigated a classical bookshelf arrangement of SmA liquid crystal confined between parallel boundary plates and subjected to a pressure gradient, as outlined in section 2 and shown schematically in Figure 2. The nonlinear dynamic equations for the steady state version of this problem were also derived in section 2. These complex coupled equations were then linearized in section 3 in order to gain insight into potentially significant behavior or boundary layer effects. The linear solutions were solved exactly and these explicit solutions allowed the identification of the two length scales L_1 and L_2 stated in (3.22). The length scale L_1, which is related to the boundary layer width identified around regions (I) and (II) in section 4, has also been identified via the classical dynamic theory for SmA liquid crystals [12]. However, the more recent dynamic theory for SmA developed in [33] allows a more sophisticated model of boundary layer effects and led to the identification of a novel second length scale, L_2, which is expected to be of an order of magnitude smaller than L_1, estimated from solutions to the linear equations.

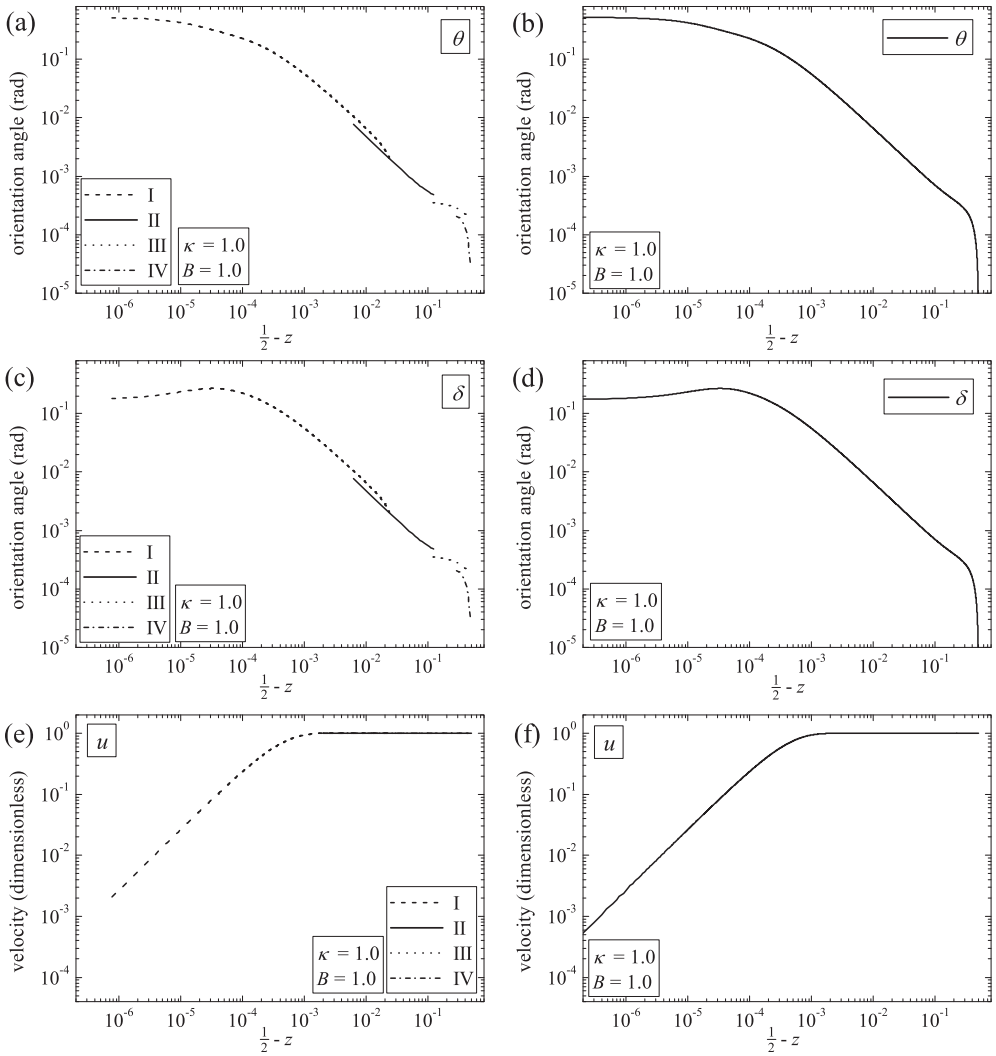

FIG. 10. *The figures on the left are derived from the asymptotic results discussed in the text for the four key layer regions identified in Figure* 9*, whereas those on the right are from direct numerical computations, all taken as functions of* $\frac{1}{2} - z$ *and for the fixed parameter values* $\kappa = 1$ *and* $B = 1$. (a) *and* (b) *show* θ, (c) *and* (d) *show* δ, *and* (e) *and* (f) *show* u.

Motivated by the identification of at least two possible length scales for differing boundary layer phenomena that arose from the solutions to the linearized problem, an investigation of the nonlinear equations was carried out in section 4 that was guided by these preliminary results. Four regions, including a primary and a secondary boundary layer, were identified by means of asymptotic analysis and have been summarized qualitatively in Figure 9. These regions were confirmed by numerical solutions to the nonlinear equations for the SmA orientation angles θ and δ and flow component u; comparisons between the asymptotic and numerical results were shown in Figure 10 for fixed values of the material control parameters κ and B. The behavior of θ, δ, and u as κ and B were allowed to vary was shown in Figure 11; these solutions were derived numerically from the full nonlinear equations. The behavior was shown to

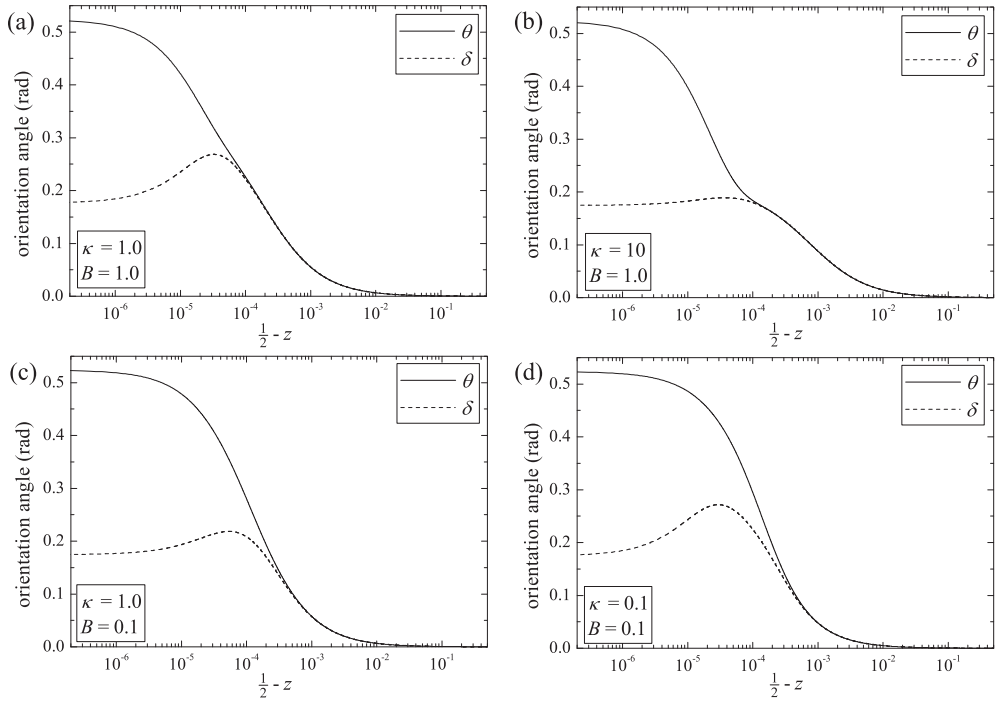

FIG. 11. *Numerically derived solutions to the dynamic problem for θ and δ as functions of $\frac{1}{2} - z$ with $\lambda_p = 10^{-16}$.* (a) $\kappa = 1, B = 1$; (b) $\kappa = 10, B = 1$; (c) $\kappa = 1, B = 0.1$; (d) $\kappa = 0.1, B = 0.1$.

be particularly sensitive to changes in the parameters κ and B around the boundary layer regions (I) and (II), as is evident in the figure. The qualitative features of the graphs in Figure 11 are very similar to those displayed for the static version of this dynamic problem that have been discussed previously [32]. A comparison between the dynamic and static versions of the orientation angles for this problem was made in Figure 12. The effect of flow was more evident near the center of the sample around the regions (III) and (IV) that were identified by an asymptotic analysis and confirmed numerically.

Elston [17] used an experimental set-up to examine the static solutions of a bookshelf-type problem for SmA, analogous to the set-up discussed in this article. He found that the smectic layer reorientation for samples of the liquid crystal SCE12 with a surface pretilt of $\theta_0 = \pi/6$ (as used in the calculations for Figure 6 and Figures 9 to 12 above) occurred over a boundary layer with a width of around $0.5\,\mu$m close to the boundary. For the rescaled length introduced here via (4.5) with $d = 10^{-5}\,$m, $0.5\,\mu$m corresponds to a dimensionless length scale of 5×10^{-2}, which clearly matches the length scale that reaches from the boundary to region (III) in Figures 9 to 12. This length scale over which the smectic layers reorient (via δ) to an idealized bookshelf alignment therefore approximately corresponds to a physical width of the same order of magnitude as that observed experimentally by Elston; this result also agrees with the results reported by Bonvent et al. [5]. The results presented in this article advance the insight of the earlier work by de Gennes [11] and, more importantly, quantify his results in the wider context of nonlinear boundary layer phenomena.

Other geometrical set-ups for similar steady state problems can be constructed and the boundary layer phenomena investigated. Preliminary studies of cylindrical

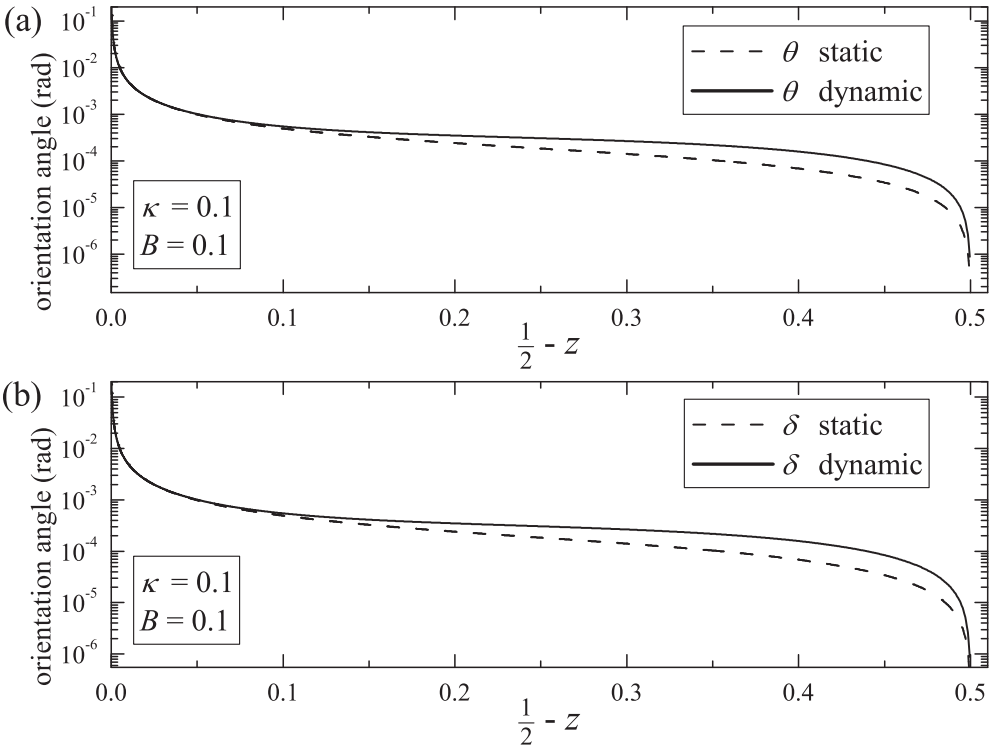

FIG. 12. *A comparison of the results for θ and δ for the steady state dynamic problem in Figure* 11(d) *with the results for the static problem derived in* [32, Figure 10(d)].

Couette flow and Poiseuille flow of SmA have been made by Walker and Stewart [37, 38] and these, together with the results in this article, can provide impetus for future investigations of boundary layer phenomena. Of particular interest would be a future study based on a recently revised version of the SmA bulk energy that has been constructed by De Vita and Stewart [15], which is of direct relevance to the modeling of lipid bilayers, based on the work of May [23]. To quadratic order in gradients, and under certain restricted symmetries, this revised energy coincides with that presented here in (2.14); however, it allows for more complex nonlinear effects to be considered as well as different symmetry conditions which may be of interest in the modeling of biological lamellar systems.

Appendix A. Consider (4.17) and (4.18) when $\varepsilon \gg 1$. We require to solve

$$\frac{\mathrm{d}^2}{\mathrm{d}z^2}\sin\theta = 0, \tag{A.1}$$

$$\frac{\mathrm{d}}{\mathrm{d}z}\left(\cos^3\delta\frac{\mathrm{d}^2}{\mathrm{d}z^2}\sin\delta\right) = 0 \tag{A.2}$$

subject to

$$\delta = \pm\delta_0, \quad \theta = \pm\theta_0 \quad \text{at } z = \pm 1/2, \tag{A.3}$$

$$\frac{\mathrm{d}^2\delta}{\mathrm{d}z^2} = 0 \quad \text{at } z = 0. \tag{A.4}$$

For θ, we have just

$$\sin\theta = 2z\sin\theta_0\,. \tag{A.5}$$

For δ, we have

$$\cos^3\delta\frac{\mathrm{d}^2}{\mathrm{d}z^2}(\sin\delta) = C, \tag{A.6}$$

where C is a constant to be determined. Also,

$$\cos^3\delta\left[-\sin\delta\left(\frac{\mathrm{d}\delta}{\mathrm{d}z}\right)^2 + \cos\delta\frac{\mathrm{d}^2\delta}{\mathrm{d}z^2}\right] = C, \tag{A.7}$$

which will imply

$$-\cos^3\delta(0)\sin\delta(0)\left[\delta'(0)\right]^2 = C. \tag{A.8}$$

Clearly, if $\delta(z) = -\delta(-z)$, then we will simply arrive at $C = 0$ and $\sin\delta = 2z\sin\delta_0$ and the question is, are there any other solutions? If there is another solution, then it cannot be antisymmetric and we must have $C \neq 0$, as well as $\delta(0) \neq 0$. Setting $Y = \sin\delta$, we obtain

$$Y'' = \frac{C}{(1-Y^2)^{3/2}} \tag{A.9}$$

subject to

$$Y(\pm 1/2) = \pm\sin\delta_0, \tag{A.10}$$

$$Y'' + YY'^2/\left(1-Y^2\right) = 0 \text{ at } z = 0. \tag{A.11}$$

Equation (A.9) can be integrated once, after multiplying by Y', to give

$$\frac{1}{2}Y'^2 = \frac{CY}{(1-Y^2)^{1/2}} + D, \tag{A.12}$$

or, alternatively,

$$\frac{1}{2}\cos^2\delta\left(\frac{\mathrm{d}\delta}{\mathrm{d}z}\right)^2 = C\tan\delta + D, \tag{A.13}$$

where D is a further constant of integration. However, there seems to be little more that can be done analytically, but it is straightforward to solve (A.9) numerically, subject to (A.10), for different values of C to see what is happening. Figure 13(a) shows δ as a function of z for $C = -1, 0, 1$ and Figure 13(b) shows $\delta''(0)$ as a function of C; clearly, the requirement that $\delta''(0) = 0$ necessitates $C = 0$.

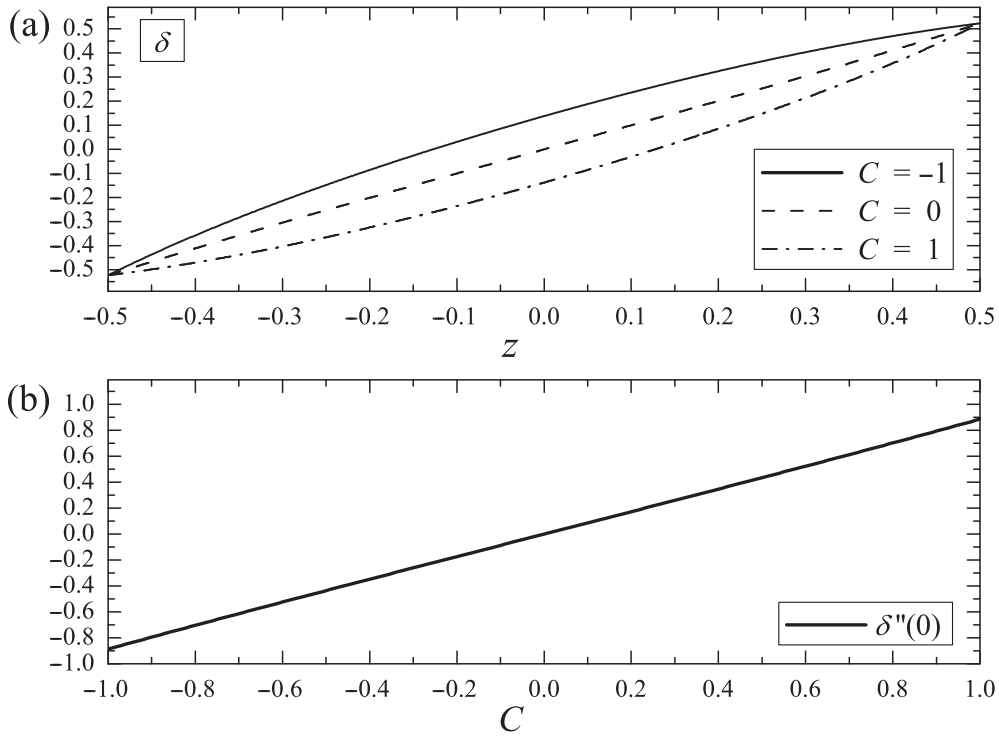

FIG. 13. (a) *The dependence of* δ *on* z *for* $C = -1, 0, 1$. (b) *The dependence of* $\delta''(0)$ *on* C.

REFERENCES

[1] G. K. Auernhammer, H. R. Brand, and H. Pleiner, *The undulation instability in layered systems under shear flow—a simple model*, Rheol. Acta, 39 (2000), pp. 215–222.

[2] G. K. Auernhammer, H. R. Brand, and H. Pleiner, *Shear-induced instabilities in layered liquids*, Phys. Rev. E, 66 (2002), pp. 061707–1–061707–14.

[3] R. Bartolino and G. Durand, *Permeative and hydroelastic flow in smectic A liquid crystals*, J. Physique, 42 (1981), pp. 1445–1451.

[4] G. K. Batchelor, *An Introduction to Fluid Dynamics*, Cambridge University Press, Cambridge, UK, 2000.

[5] J. J. Bonvent, J. A. M. M. van Haaren, G. Cnossen, A. G. H. Verhulst, and P. van der Sluis, *Pretilt angle measurements on smectic A cells with chevron and tilted layer structures*, Liquid Crystals, 18 (1995), pp. 723–731.

[6] M. Cagnon and G. Durand, *Mechanical shear of layers in smectic-A and smectic-B liquid crystal*, Phys. Rev. Lett., 45 (1980), pp. 1418–1421.

[7] W. K. Chan and W. W. Webb, *Determination of the permeation coefficient in a lyotropic smectic liquid crystal by annealing elementary edge dislocations*, Phys. Rev. Lett., 46 (1981), pp. 603–606.

[8] S. Chandrasekhar, *Liquid Crystals*, 2nd ed., Cambridge University Press, Cambridge, UK, 1992.

[9] N. A. Clark, *Observation of extended boundary layers in the permeative flow of a smectic-A liquid crystal around an obstacle*, Phys. Rev. Lett., 40 (1978), pp. 1663–1666.

[10] P. A. Cruz, M. F. Tome, I. W. Stewart, and S. McKee, *A numerical method for solving the dynamic three-dimensional Ericksen–Leslie equations for nematic liquid crystals subject to a strong magnetic field*, J. Non-Newtonian Fluid Mech., 165 (2010), pp. 143–157.

[11] P. G. de Gennes, *Viscous flow in smectic A liquid crystals*, Phys. Fluids, 17 (1974), pp. 1645–1654.

[12] P. G. de Gennes and J. Prost, *The Physics of Liquid Crystals*, 2nd ed., Oxford University Press, Oxford, UK, 1993.

[13] R. De Vita and I. W. Stewart, *Influence of weak anchoring upon the alignment of smectic A liquid crystals with surface pretilt*, J. Phys. Condensed Matter, 20 (2008), pp. 335101–1–335101–9.
[14] R. De Vita and I. W. Stewart, *Nonlinearities in tilt and layer displacements of planar lipid bilayers*, Eur. Phys. J. E, 32 (2010), pp. 319–326.
[15] R. De Vita and I. W. Stewart, *Energetics of lipid bilayers with applications to deformations induced by inclusions*, Soft Matter, 9 (2013), pp. 2056–2068.
[16] W. E, *Nonlinear continuum theory of smectic-A liquid crystals*, Arch. Ration. Mech. Anal., 137 (1997), pp. 159–175.
[17] S. J. Elston, *The alignment of a liquid crystal in the smectic A phase in a high surface tilt cell*, Liquid Crystals, 16 (1994), pp. 151–157.
[18] W. Helfrich, *Capillary flow of cholesteric and smectic liquid crystals*, Phys. Rev. Lett., 23 (1969), pp. 372–374.
[19] A. Jákli and A. Saupe, *Field-induced thickness change of ferroelectric liquid crystal films*, Phys. Rev. E, 53 (1996), pp. R5580–R5583.
[20] M. Kléman and O. D. Lavrentovich, *Soft Matter Physics: An Introduction*, Springer-Verlag, New York, 2003.
[21] G. J. Krüger, *Diffusion in thermotropic liquid crystals*, Phys. Rep., 82 (1982), pp. 229–269.
[22] F. M. Leslie, I. W. Stewart, and M. Nakagawa, *A continuum theory for smectic C liquid crystals*, Mol. Cryst. Liq. Cryst., 198 (1991), pp. 443–454.
[23] S. May, *Protein-induced bilayer deformations: The lipid tilt degree of freedom*, Eur. Biophys. J., 29 (2000), pp. 17–28.
[24] C. W. Oseen, *The theory of liquid crystals*, Trans. Faraday Soc., 29 (1933), pp. 883–899.
[25] S. V. Pasechik and A. V. Torchinskaya, *Behaviour of nematik layer oriented by electric field and pressure gradient in the striped liquid crystal cell*, Mol. Crys. Liq. Cryst., 331 (1999), pp. 341–347.
[26] S. V. Pasechnik, A. V. Torchinckaya, B. A. Schustrov, and T. N. Jurmanova, *Nonlinear optical response of nematic liquid crystal on varying pressure difference in the presence of electric field*, Mol. Crys. Liq. Cryst., 367 (2001), pp. 727–734.
[27] R. Ribotta and G. Durand, *Mechanical instabilities of smectic-A liquid crystals under dilative or compressive stresses*, J. Physique, 38 (1977), pp. 179–204.
[28] A. N. Shalaginov, L. D. Hazelwood, and T. J. Sluckin, *Dynamics of chevron structure formation. II. Permeation-dominated phenomena*, Phys. Rev. E, 60 (1999), pp. 4199–4209.
[29] T. Soddemann, G. K. Auernhammer, H. Guo, B. Dünweg, and K. Kremer, *Shear-induced undulation of smectic-A: Molecular dynamics simulations vs. analytical theory*, Eur. Phys. J. E, 13 (2004), pp. 141–151.
[30] F. Stewart and I. W. Stewart, *A novel method for measuring compression constants in smectics*, Mol. Cryst. Liq. Cryst., 478 (2007), pp. 23–32.
[31] I. W. Stewart, *The Static and Dynamic Continuum Theory of Liquid Crystals*, Taylor and Francis, London, 2004.
[32] I. W. Stewart, *The alignment of smectic A liquid crystals with director tilt on the boundaries*, J. Phys. A, 40 (2007), pp. 5297–5318.
[33] I. W. Stewart, *Dynamic theory for smectic A liquid crystals*, Contin. Mech. Thermodyn., 18 (2007), pp. 343–360.
[34] I. W. Stewart and F. Stewart, *Shear flow in smectic A liquid crystals*, J. Phys. Condensed Matter, 21 (2009), pp. 465101–1–465101–13.
[35] E. G. Virga, *Variational Theories for Liquid Crystals*, Chapman and Hall, London, 1994.
[36] A. J. Walker, *The alignment of cylindrically layered smectic A liquid crystals with director tilt on the boundaries*, J. Phys. A, 41 (2008), 385205.
[37] A. J. Walker and I. W. Stewart, *Couette flow of a smectic A liquid crystal*, J. Phys. Condensed Matter, 21 (2009), 155101.
[38] A. J. Walker and I. W. Stewart, *Poiseuille flow of a smectic A liquid crystal*, Internat. J. Engrg. Sci., 48 (2010), pp. 1961–1970.
[39] H. G. Walton, I. W. Stewart, and M. J. Towler, *Flow past finite obstacles in smectic liquid crystals: Permeative flow induced S_A to S_C phase transition*, Liquid Crystals, 20 (1996), pp. 665–668.
[40] D. G. Zill and M. R. Cullen, *Advanced Engineering Mathematics*, 2nd ed., Jones and Bartlett, Sudbury, MA, 2000.